2019

Thévenin Equivalent of Solar Cell Model

Chiedozie Osigwe
Minnesota State University, Mankato

Thévenin Equivalent of Solar Cell Model

by

Chiedozie Osigwe

A Thesis Submitted in Partial Fulfillment of the

Requirements for the Degree of

Master of Science

In

Electrical Engineering

Minnesota State University,Mankato

Mankato,Minnesota

December 2019

December 6th, 2019

Thévenin Equivalent of Solar Cell Model

Chiedozie Osigwe

This thesis has been examined and approved by the following members of the student's committee.

Professor Vincent Winstead, P.E
Advisor

Associate Professor Nannan He
Committee Member

Assistant Professor Jianwu Zeng
Committee Member

Dedication

To GOD almighty for the guidance, protection, strength and health granted to me.

"Never be afraid to trust an unknown future to a known God."$_{-CorrieTenBoom}$

To my parents, S.N Osigwe and P.E Onyenemezu, my brother and his family, my sister, Onyenemezu family and dear friends, who have been a source of inspiration, strength, advice, encouragement and support(financially, morally and emotionally).

"Other things may change us, but we start and end with family"$_{-AnthonyBrandt}$

To the faithful departed - Brian Blum, Chukwuma Omeokwe.

"I talk to God but the sky is empty"$_{-SylviaPlath}$

Acknowledgment

It is with a heart full of gratitude, i wish to express my deepest appreciation to my academic advisor and mentor Professor Vincent Winstead for guiding me through my program. Honestly, words can not fully describe.

"teacher for a day, father for a life time."$_{-ChineseIdiom}$

I humbly thank my committee Professors and all my professors whom i have had the privilege of working with, your advice and guidance is immeasurable.

"Whoever undertakes to set himself/herself up as a judge of truth and knowledge is ship wrecked by the laughter of the gods"$_{-EdmundBurke}$

Special thanks to James Gullickson, Karen Wright, Kiondo Lyn, friends and colleagues for your unwavering encouragement and support.

Abstract

This thesis considers the problem of determining impedance parameters of a solar cell in operation. Typically, solar cell devices are characterized by the manufacturer using empirical data prior to placing the solar cell in use. There are a number of solar cell degeneration mechanisms that are of interest to measure or detect. Therefore, active measurement of solar cell impedance parameters periodically over time is advantageous. We propose a methodology developed from a Thévenin equivalent model of a typical solar cell. This method allows periodic updating of the solar cell's parameters which can be used to update the cells characterization and/or monitor degradation of the cell.

Contents

List of Figures

List of Parameter Definitions

G - Solar irradiance

G_n - Nominal solar irradiance at 1000W/m^2

T - Temperature of cell/module in Kelvin

T_n - Nominal Temperature

k_i - Temp. coefficient of current.

I_{sc} - Short circuit current of the cell at reference temperature

I - Output current of cell/module

I_{ph} - Photo current

I_d - Diode saturation current

R_s -Series resistance

R_{sh} - Shunt resistance

I_{sh} - Current through shunt resistor

I_s - Reverse saturation current at reference temperature

I_{mp} - Current at Maximum power condition

P_m - Maximum power

V - Terminal voltage of the cell/module

V_{oc} - Open circuit voltage at reference temperature.

V_{mp} - Voltage at Maximum power condition

V_t - Thermal voltage of cell/module at reference temperature

q - Electron charge = 1.6 x 10^{-19}C

N_s - Number of connected cells

K - Boltzman's constant = 1.3805 x 10^{-23}J/K

N - Diode ideality factor

P – Output power of the cell/module

η - Efficiency of the cell/module.

A_c - Area of the cell/module (m^2).

E_{th} - Input light energy (W/m^2) or Ambient Irradiation

K_i - Short circuit current co-efficient in $A/^0C$

E_g - Band gap energy in electron volt

Chapter 1

Introduction

Energy generation has been at the forefront of the modern world whereas traditional energy sources have been derived from oil and gas. Over the years, an increase in demand for energy has seen a rise in fossil fuels combustion and, subsequently, carbon emissions which affects our climate globally. Recently this trend is changing as fossil fuel based generation of electricity, for example, is being phased out and replaced by renewable resources. However, fossil fuel usage is still substantial.

Due to these effects, renewable energy such as solar power, wind power, ocean currents and the use of bio-fuels are promising alternatives to traditional energy generation for the purpose of positively impacting the global climate by reducing the effects of carbon emissions. One of the common applications of renewable energy for electrical power generation is through the use of solar panels over large areas referred to as solar farms.

Recent advances in solar cell technology development have led to incremental increases in panel voltages and cell current along with efficiency gains. Similar to other methods of electric power generation, solar cells have loss mechanisms, one of which is the series resistance loss limiting the performance of the cell which can be

measured and detected Degenerative mechanisms, such as the ohmic series resistance loss which affects the internal series resistance and shunt resistance, typically arises from the resistance within the device itself [1]. Due to this, derivations of equivalent circuits for solar cells have been used to model and measure the effects of these internal losses [1–3]. Usually, solar cell devices are characterized by the manufacturer using empirical data prior to the solar cell being encapsulated in a panel.

Over the years the awareness of renewable energy and its applications has led to significant increases in the photovoltaic industry. Furthermore, these advances have directly led to advanced research and enhanced industrial processes. Wherein future concepts as stated by V.Winstead et al[50] can be implemented, such as combining thin film solar cells like CIGS with wind turbine blades to increase power production.

Chapter 2

Photovoltaic Energy

Photovoltaic energy is harnessed from the result of the direct transformation of solar radiation into electrical energy, by means of a photovoltaic cell. In this chapter we consider the development of solar cell technology. That is, a summary of the technology that drives the photovoltaic systems currently in production. To understand solar irradiance to electricity conversion and properties of these cell materials we consider the underlying fundamental physics.

Conversion of solar energy into electrical energy works on the principle of photoelectric effect, which is the ability of photons to create charge carriers (electrons and holes) in a material. Along with further advancements in semiconductor technology, there has been a considerable leap in the photovoltaic industry, in terms of better raw materials for solar cells/panels and enhanced manufacturing processes which has seen an increase from the 6% energy conversion efficiency of earlier silicon based cells [4, 5] to the currently produced cells of 17% - 20% efficiency used in today's photovoltaic system[5].

The photovoltaic cell, also called solar cell, can be manufactured using semiconductor materials similar to the manufacture of transistors or microchips in a computer.

The photovoltaic technology most used since the creation of the first cells has been the crystalline-type silicon. Most photovoltaic cells are usually made of "crystalline silicon" since Silicon is one of the most abundant elements on Earth under non-toxic silica form and cheaper to process. Hence, making it a cost effective resource. Currently silicon-based cell technology is not the only one to participate in the world production of solar cells,there are also Thin Film, Concentrated Photovoltaic(CPV) and Organic Material. Therefore, PV technology is usually classified into three generations depending on the base material used. [6]

2.1 Solar Resource

Solar energy is the most abundant renewable resource in the world being named from it's source. In photovoltaic systems, the knowledge of the sun is critical in it's operation and optimization. Several factors such as time, season of the year, landscape, weather, and geographical location affects the amount of sunlight received by the surface of the earth. Since the earth is round, the angle of incidence on a given surface of the earth will depend on the orientation of the earth and the intensity of the ray will depend on the distance that the light has to travel to reach the surface. this is also known as air mass concept [7].

The latitude, time and season varies due to the rotation and inclination of the earth. Also, atmospheric bodies such as clouds, particles, fog and various other meteorological phenomena, cause hourly and daily variations that sometimes increase or sometimes diminish the solar radiation and make it diffuse. This is usually experienced fully during seasonal changes. To harness this energy or solar radiation, several factors are considered like the earth's orbit; angle of the device and solar time to mention a few. Solar systems are designed and analyzed through straightforward

but complicated sets of equations to capture and predict some of the factors and the sun's intensity [8].

2.1.1 Solar Spectrum

The solar spectrum is characterized in terms of emitted energy using the air mass concept. The Sun emits electromagnetic radiation, which has a wavelength band varying from 0.22μm, which is in the ultraviolet band, to 3μm which is in the infrared band. Figure 2.1 below represents the variation in the energy spectral distribution. This is different from the spectrum outside the atmosphere which closely resembles black body radiation. The energy associated with this solar radiation can be split into approximately three bands:

- 7% in the ultraviolet band ($< 0.4\mu$m),
- 47% in the visible band (0.4 to 0.8μm),
- 46% in the infrared band ($> 0.8\mu$m).

The Earth's atmosphere receives this radiation at an average power of 1.37 kilowatt per square meter (kW/m^2) approximately, in the space outside the Earth's atmosphere, depending on whether the Earth is moving away or approaching the sun during its rotation around it. As the solar radiation approaches the earth atmosphere some it is absorbed by various constituents. This gives the spectrum its irregular shape, so that the amount of energy reaching the Earth's surface seldom exceeds 1.2kW/m^2 (1200W/m^2). The energy available at a given point on earth varies according to how much of the atmosphere the radiation passes through to get to the surface. This can be expressed with the airmass ratio (equation 2.1) [8].

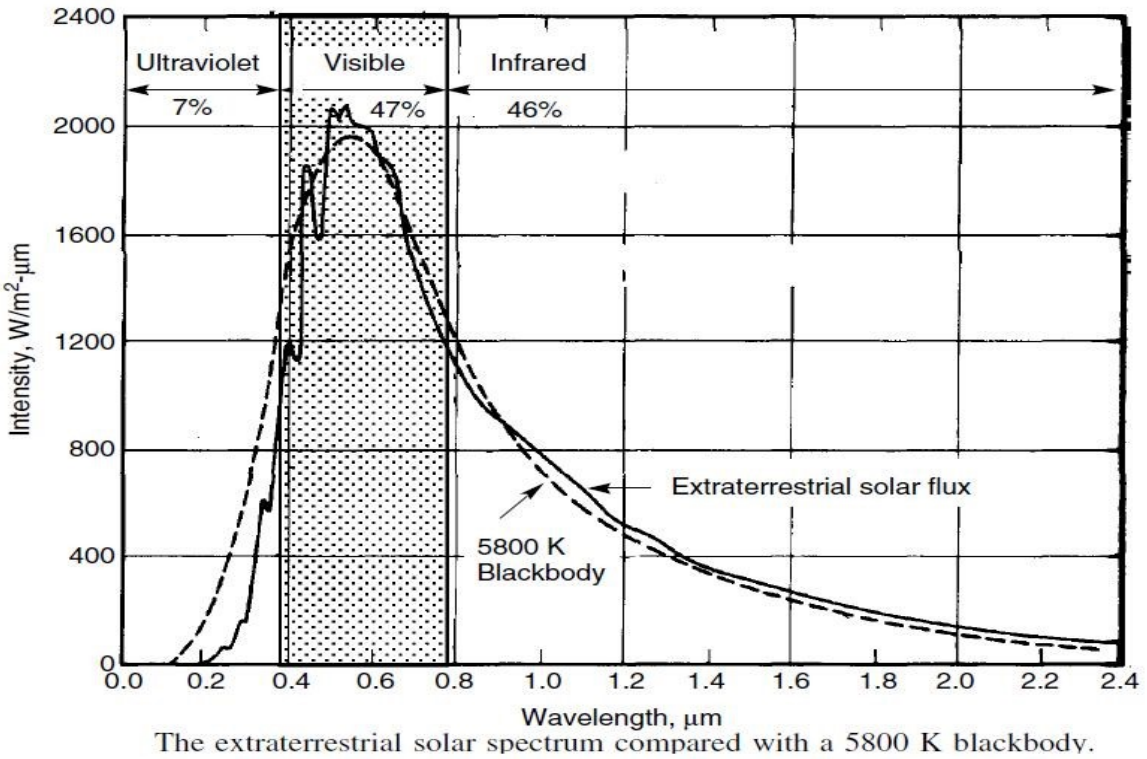

Figure 2.1: Extraterrestrial solar spectrum [8]

$$m = \frac{h_1}{h_2} = \frac{1}{sin\beta} \tag{2.1}$$

where,

- h_1 is the path length through the atmosphere with the sun directly above.
- h_2 is the path length through the atmosphere to reach a spot on the surface.
- β is the angle of inclination of the earth.

2.1.2 Standard conditions

Two different spectral distributions have been defined for the sun. the AM0 spectrum relates to radiation in outer space and the AM1.5 G spectrum is at sea level with

certain standard conditions. Uniform conditions are usually specified so that performance can be compared between different PV units. The parameters obtained from testing are usually provided on the manufacturers data sheet[9] while the measurements performed and the electrical characteristics obtained under the standard test conditions accurately characterizes the photovoltaic modules.

The standard conditions for the qualification of photovoltaic modules are:

- A specified light spectral distribution with an Air mas, AM = 1.5;
- A vertical irradiance of 1000W/m^2;
- A reference cell temperature of 25^0C with a tolerance of $\pm 2^0$C

Air mass figures provide a relative measure of the path the sun must travel through the atmosphere. The manufacturers of solar panels specify the performance of their equipment under the standard conditions mentioned above (S.T.C: standards test conditions). In addition they also provide performance data under the Nominal Operating Cell Temperature.(NOCT) [1, 7, 10].

2.2 Photovoltaic Conversion

The Photovoltaic conversion of solar energy refers to electricity produced by transforming part of the solar radiation with a photovoltaic cell. Photovoltaic cells directly convert the light energy into electricity (low voltage direct current). In most cases, several cells are interconnected in series and/or parallel to form a solar panel (or photovoltaic module).

2.2.1 Photovoltaic cell operation

The photovoltaic effect is a physical phenomenon or technology, which converts light (photons) into electricity using a semiconductor material; for example crystalline silicon. The latter has special electronic properties. To form a photovoltaic cell it is necessary, from this material, to form a junction with an upper layer exhibiting an excess of electrons (doped zone n) and a lower layer with an electron deficiency (doped zone p).

When a photon is absorbed by the material, it passes part of its energy by collision to an electron literally tearing it from the material. The latter, being previously at a lower energy level where it was in a stable state, will then pass to a higher energy level, creating an electrical imbalance within the material. This results in the creation of an electron-hole pair, yielding a flow of electrical current.

Conversely, from Figure 2.2, the exposure of the semiconductor to solar radiation will create an excess of electrical charges in both layers. Joining together two different electronic material property will cause an electric field. Likewise, all the energy of the photons that cannot be converted into electricity is absorbed by the material in thermal form. The material constituting the PV effect then experiences internal temperature increases proportional to the solar energy received. The thermal effect is therefore a leading cause of performance deterioration in solar cells [11].

Photovoltaic Advantages

The advantage of the Photovoltaic systems are apparent in places with out grid electricity and where internal combustion engines are expensive to operate. Not withstanding, the Photovoltaic powered systems have; 1) No combustion fuels and fumes, 2) Low maintenance, 3) Unattended Operation, 4) Easy to install, 5) Low

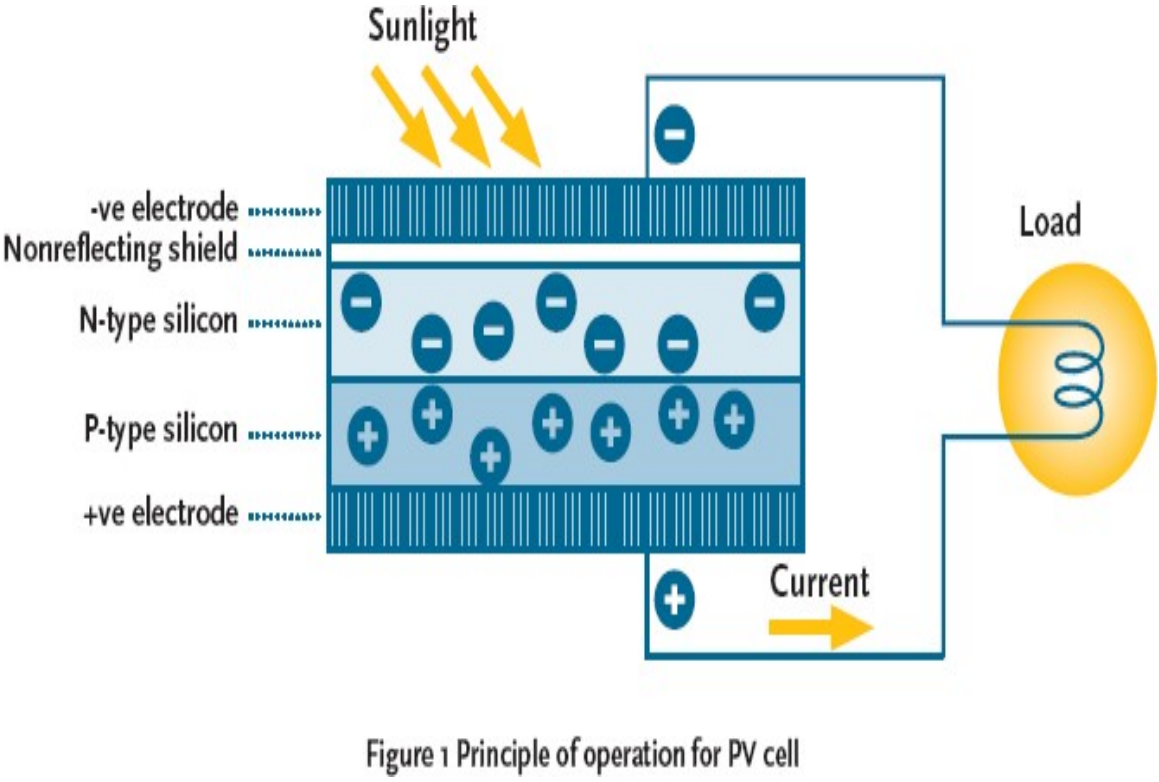

Figure 2.2: Operation of a Photovoltaic cell [12]

recurrent costs, 6) Reliable long life[5]. They can be used in PV powered pumps, streetlights, house holds, etc.

2.2.2 Photovoltaic technology

Photovoltaic cell manufacturers have, over time, developed different panels based on a variety of materials that make up several types of modules. The understanding of each technology and its associated challenges will provide a suitable basis to recognize advantages and drawbacks. PV cell technologies are usually classified into three groups or generations. Although in this thesis we will be specifically considering the crystalline silicon panels.

Crystalline Silicon

The energy that an electron must acquire to jump across different bands is called the band-gap energy. Silicon is a semi conductor material with a band gap of 1.1ev which is suitable for PV applications. Crystalline Silicon(C-Si) is the material used commonly in Photovoltaic panels.

a) Mono-crystalline Silicon: Mono-crystalline Silicon cells represent the first generation of photovoltaic generators. See Figure 2.3. To make them, Silicon silica is melted. During a slow and controlled cooling, Silicon (metallurgical MG-SI) solidifies by forming only one crystal (so-SI Solar Silicon) of large size (in the form of a bar). The crystal is then cut into thin slices that are used for individual cells. These cells are generally characterized by a uniform blackish hue color [8, 11].

Figure 2.3: Mono-crystalline silicon solar cell [13]

b) Poly-crystalline Silicon: The Silicon molecular structure originates from the cooling stage of Silicon in a mold, leading to the formation of several groups of crystals. The silicon is cast in blocks. When it hardens it results in a structure of different sizes where border defects occur [14]. This silicon cell is often of bluish hue color in appearance, but not uniform. One can distinguish motifs created by the different crystals. See Figure 2.4.

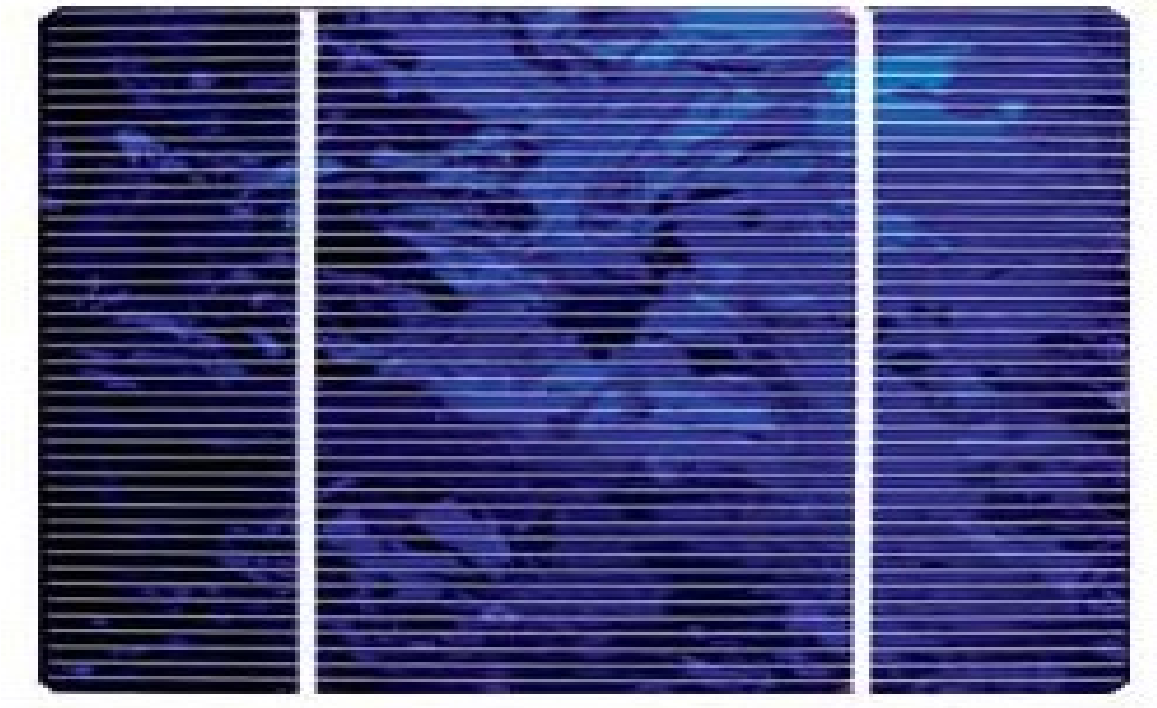

Figure 2.4: Poly-crystalline silicon solar cell [13]

Both mono-crystalline and poly-crystalline solar panels serve the same function in the overall solar PV system; they capture energy from the sun and turn it into electricity. Many solar panel manufacturers produce both mono-crystalline and poly-crystalline panels. Both mono-crystalline and poly-crystalline solar panels can be good to use for different applications, but there are some differences between the two types of technology such as the type of silicon solar cell they use. That is, mono-

crystalline solar panels have solar cells made from a single crystal of silicon, while polycrystalline solar panels have solar cells made from many silicon fragments melted together.

c) Ribbon Silicon: String ribbon Silicon is grown by a vertical sheet growth technique developed by evergreen solar [15]. The process entails long strings being unwound from spools. The melt is replenished and the silicon ribbon is cut to length for further processing, without interrupting growth. This technique produces low cost Silicon due to high silicon feed back stock utilization. Initially developed at 300μm thickness, further research and development have been able to propose a 100μm thickness which improves its cost of production and efficiency.

Thin Film

This can be said to be a variant of the multi-crystalline technology where the silicon manufactured is deposited on one or more semi-conductive or photosensitive layers in a continuous process onto a base material such as glass, plastic, polymer,etc., giving a fine grained sparkling appearance. This technology reduces the cost of manufacturing, but its yield is lower than that of crystalline silicon cells. In addition, thin films, due to their thickness, can be utilized in flexible light-weight structures that can be used in building components such as building integrated photovoltaic(BIPV). There are different variants of thin film solar cells that have been commercially made namely;

a) Amorphous Silicon: The Silicon cells are are made by depositing Silicon in a thin homogenous layer on to a substrate(flexible or rigid) rather than creating a rigid crystal structure. The substrate can be flexible or rigid which gives it a wide range of applications such as curved surfaces or bonding directly on roof surfaces. However, crystalline technology has a higher efficiency than it. See Figure 2.5 for an example.

b) Cadmium Telluride: This material is a poly-crystalline semiconductor com-

Figure 2.5: Amorphous silicon solar cell

pound made of Cadmium and Tellurium. During the manufacturing process a Cadmium sulfide film is grown either by chemical bath, chemical vapor deposition or vapor transport deposition[5]. While their efficiency is lower than crystalline silicon, they tend to be easier to mass produce since for thin films, less materials are needed for production.

c) Copper Indium selenide(CIS) and Copper Indium Galllium-Diselenide(CIGS): The objective of exploring different compounds made up of several elements is to find possible combinations of band-gap that approaches the optimal value of 1.4ev while minimizing inefficiencies. CIGS is a polycrystalline semiconductor compound of Copper,Indium and Selenium. The CIS PV cells offer the highest efficiencies in this category of thin film technology [16]. It is a material that shows high energy conversion efficiency and lacks outdoor degradation problems.

Figure 2.6: Thin film solar cell

Various Technologies

This section discusses Photovoltaic technologies that have been theorized but not yet been implemented in whole sale commercial use. However PV technologies like the dye-sensitive solar cell and organic solar cell have been commercialized.

a) Dye-Sensitized Solar Cell (DSSC): are a promising third-generation photovoltaic technology due to their ease of fabrication, low cost, ability to operate in diffused light, flexibility, and light weight. In DSSCs, solar cells use photo-electrochemical solar cells which are based on semiconductor structures formed between a photosensitive anode and electrolyte. The counter electrodes play a critical role in electrocatalytic reduction where the redox electrolyte collects and transfers the electrons from the external circuit. Typically the nano-crystals serve as antenna that harvest

the sunlight while the dye molecule separates the charge. [14, 17]

b) Organic Solar cell (OSC): These cells are manufactured from the only solar cell technology that fully addresses the challenges of manufacturing on a scale corresponding to an energy production capacity of 1 GW peak per day based solely on abundant elements. This ability arises through the use of printing techniques and photo active layers comprising carbon-based conjugated polymer materials. The technology is briefly reviewed in this chapter by describing its common device structures and materials [18].

Distinguishing the PV technologies through these categories is not exhaustive as future trends in PV technology is evolving and growing. Examples include Concentrating Photovoltaic Technology(CPV) and black silicon cells.

2.3 Photovoltaic Encapsulation

Solar cells are usually thin sheets of semiconductor material made up from a single crystal or multi-crystal ingot while the thin films are basically continuous layers of semi-conducting material deposited on a substrate or a superstrate by chemical vapor deposition techniques[19]. Hence the thickness of these cells are little therefore due to the fragile nature of the solar cells it is essential that the cells are protected and supported. A solar cell module usually comprises of the support mechanism, the superstrate and substrate in addition the cells are covered with an encapsulant as shown in Figure 2.7. There are different methods of encapsulation depending on the material used such as Lamination encapsulation which is the most common, Resin transfer, Silicon encapsulation and Vacuum bagging [19].

Generally, the most widely used encapsulant materials like the Ethylene Vinyl Acetate(EVA), silicone and urethane have to be subjected to a chemical crosslink-

ing process which can be induced by high temperature levels or UV irradiation. The thermoplastic materials like Polyvinyl butyra(PVB), thermoplastic polyolefin elasomer(TPSE) and ionomers, as well as modified polyolefines (PO), melt during the module manufacturing process without formation of chemical bonds (crosslinks) between the polymer chains [20]. The encapsulant material strongly adheres to all surfaces binding the components mechanically into a laminate. the encapsulants should be able to inhibit leakage currents that may arise due to rain or dew wetting by having a high level resistivity to avoid potential induced degradation [21].

Encapsulation is needed to protect solar cells from moisture and other external elements while providing electrical and optical transitivity. Additionally it boosts durability and ensures reliability of the cells.

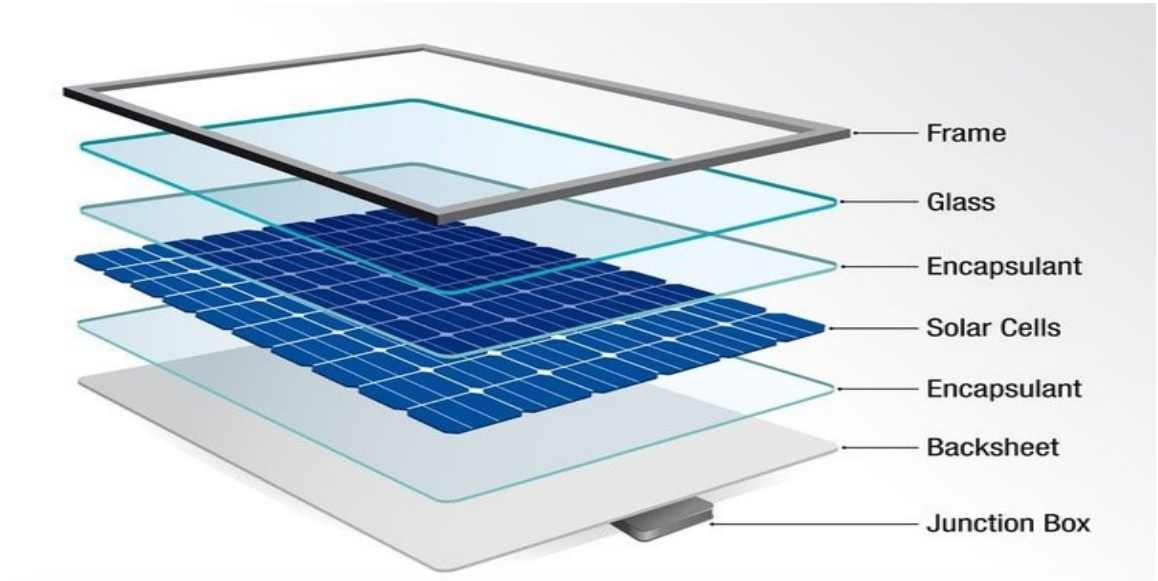

Figure 2.7: Solar cell encapsulation [20]

2.4 Photovoltaic Degradation Mechanisms

One of the major source of reliability issues in other types of electrical generating systems is the moving parts, such as motors or gears, that they have. A good advantage Photovoltaic systems have over other types of systems is the absence of such moving parts. This contributes to the photovoltaic module's long operating life. The operating life is largely determined by the stability and resistance to corrosion of the materials from which it is constructed. Manufacturer guarantees of up to 20 years indicate the quality of bulk silicon PV modules currently being produced. Nevertheless, there are several failure modes and degradation mechanisms which may reduce the power output or cause the module to fail [22].

With the prevalence of photovoltaic electrical generation as a power source for the the power grid on the rise, the ability to accurately predict power delivery over the course of time is of vital importance to the growth of the photovoltaic industry. Degradation in photovoltaic systems involves either a gradual reduction in the output power of a Photovoltaic module over time or a power reduction due to failure of an individual solar cell in the module. While degradation and failure may sound similar there exists a slight difference between the two terms. The difference being its effects on the photovoltaic system over time. Failures usually happen abruptly while degradation may be slower as seen in the figure 2.8 below, which shows the failure and reliability curve of a photovoltaic module.

2.4.1 Photovoltaic Failures

Failures of Photovoltaic equipment can stem from materials, fundamental product design flaws or failures in quality control during manufacturing. Figure 2.8 below indicates leading Photovoltaic module degradation and failure mechanisms that occur

as infant mortalities, mid-life failures, and wear out. Most of the failures that occur during the infant stage are related to glass breakage, handling, weather conditions, electrical connectors, and the junction box of the module. These factors will be described in detail next.

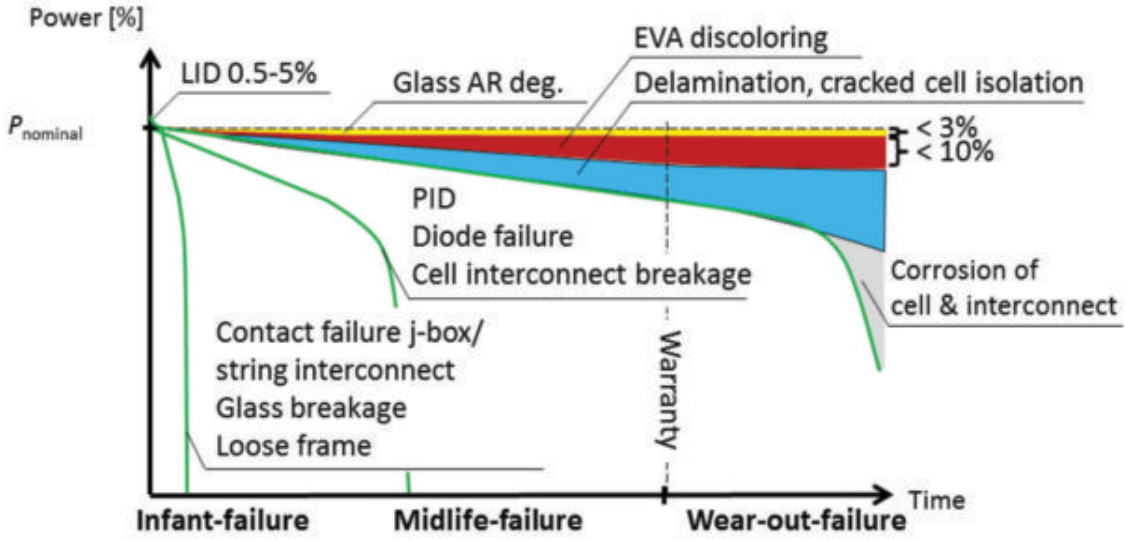

Figure 2.8: Solar cell failures and degradation [23]

Glass Breakage

Glass photovoltaic modules are more sensitive to glass breakage. The failure usually originates during the planning and installation stage either by poor clamp geometry for the module or the positions of the clamps on the module not being chosen in accordance with the manufacturer's manual or breakage from use of excessive force such as excessively-tightened screws during the mounting phase. Glass breakage leads to loss of performance in time due to cell and electrical circuit corrosion caused by the penetration of oxygen and water vapour into the PV module. Major problems caused by glass breakage are electrical safety issues. Firstly, the insulation of the modules is

no longer guaranteed, in particular in wet conditions. Secondly, glass breakage causes hot spots, which lead to overheating of the module [23].

Handling

This includes the transportation and installation of the photovoltaic modules. They are the first critical stages in a PV module's life. The glass cover of some Photovoltaic modules may break or cells in the laminate may break due to vibrations and shocks that occur during transportation or installation. In the case of glass breakage we can consider as an induced human error beyond control. However, the cause of cell breakage is much more difficult to uncover. Visually it cannot be seen and in many cases it cannot be detected by a power rating of the PV module directly after occurrence of the cell breakage. Some typical situations that may lead to cell cracks are; 1) A PV module falling over, 2) Loose bracing on transport containers, 3) An insufficiently rigid pallet touching the lowest PV module in the stack during transportation.

Weather conditions

Environmental factors may cause a Photovoltaic module to be producing reduced output or failure such as snowfall, cloudy days or heavy rainfall and shading from a growing tree. One module may fail or the interconnects between modules may have changed the operating point of the array. However, these reductions in power are all reversible, provided that the original cause is rectified. A more severe condition could arise from a lighting strike. A defective bypass diode caused by a lightning strike is caused by an external source, for which the module is not designed. Typical induced defects caused by a lightning strike are open-circuit bypass diodes or mechanical breakage of a Photovoltaic module directly hit by lightning strike. Both defect types

may cause hot spots leading to subsequent failures.

Electrical Connectors

It is of value to mention quick connectors though it is debatable whether it is a photovoltaic failure. However it is a point of failure that occurs during installation. The quick connector electrically connects solar modules to each other, to fuse boxes, to extension cables, combiner boxes and to the inverter. This element is very important for the safety and reliable power generation of the system. Low-voltage DC connectors as a special kind of contact pair are also frequently discussed in respect to electric automotive vehicles as well as Photovoltaic applications[23]. Some of the failures originate from mismatching quick connectors of different types or inaccurately fitting quick connectors to connect extension cables, fuse boxes, or the inverter at the installation site. Badly fitted connectors may result in power loss or electrical arcs [23]

Junction Box

The junction box is the container fixed on the backside of the module which protects the connection of cell strings of the modules to the external terminals. Generally the junction box contains the bypass diodes to protect the cells in a string in case of hot spot or shadowing[23]. Some of the failures that arises are: 1) Poor fixing of the junction box to the backsheet, 2) Opened or badly closed j-boxes due to poor manufacturing process, 3) Moisture ingress which cause corrosion of the connections and the string interconnects in the junction box, 4) Bad wiring causing internal arcing in the j-box. This failure is particularly dangerous because the arcing can initiate fire[23].

2.4.2 Degradation Mechanisms

As the solar industry matures, long term performance and reliability of PV modules and other system components such as inverters have received increased focus from industry. Developing an understanding of how photovoltaic modules age in the field will highlight technological risks and enable the implementation of an effective procurement. The things to note would include efficiency with which sunlight is converted into power and how long the efficient conversion is sustained. An accurate quantification of power decline over time, also known as degradation rate, is essential especially when predicting return on investment which require accurate prediction of decreased power output over time [23, 24]. Some of these mechanisms include, delamination, micro-cracks, thermal cycling, etc. These will be introduced in detail.

Delamination

Once the adhesion is compromised because of contamination such as poor bonding or improper glass cleaning or environmental factors(that is sensitivity of adhesive bonds to ultraviolet light at higher temperatures or to humidity in the field), fractures into layers will occur within the module. This effect usually would involve moisture ingress and corrosion. Delamination at interfaces within the optical path will result in optical reflection leading to power loss, loss of current from the modules, and an increase of series resistance due to the adhesion between the glass, encapsulant, active layers, and back layers being compromised[23, 25, 26].

Encapsulant Discoloration

A major degradation mechanism in photovoltaic modules is the physical change of the encapsulant, which significantly affects its performance and reliability. Ultraviolet

absorbers and other encapsulant stabilizers ensure a long life for module encapsulating materials. However, slow depletion, by leaching and diffusion does occur and once concentrations fall below a critical level, rapid degradation of the encapsulant materials occurs[25]. In particular, the highlighted discoloration that is yellowing or browning of the ethylene vinyl acetate (EVA) can occur in Silicon modules operating in certain climatic conditions. The effect of discoloration causes loss of transmittance of the encapsulant ethylene vinyl acetate(EVA), reducing the photo current (I_{ph}) of the cell module hence culminating in decreased absorption of sunlight by the photovoltaic cell module and power loss[25–27].

Snail Trail and Micro-Cracks

Snail trail is a discoloration of the panel which has been attributed to the use of defective front metallization silver paste[23] in the solar cell manufacturing process. The discoloration usually takes a number of years before it seen. Defective silver paste can lead to moisture in the panel which causes oxidation to occur between the silver paste and the encapsulation material called ethylene vinyl acetate(EVA). The snail trails can also arise as a result of microscopic cracks in the panel. These micro cracks can occur during Photovoltaic modules production, shipping, or being mishandled during installation. They are tiny microscopic tears in the solar cells. They usually happen in wafer based crystalline panels. Micro cracks do not cause any damage but over time with the influence of seasonal weather conditions they grow to larger cracks that can lead to loss of power.

Thermal Cycling

Photovoltaic modules are constructed from several materials, each with varying coefficients of thermal expansion. As ambient temperature and irradiance fluctuates,

materials expand or contract[28]. When adjacent materials have mismatched coefficients of thermal expansion (for example silicon solar cells and metal busbar ribbons), the interface experiences stress induced by the presence of higher ambient temperature along with humidity[28]. This can lead to aging such as solder joint fatigue, increases in series resistance and decreases in power.

Humidity-Freezing

Rapid changes in environmental conditions can attribute to degradation especially in regions of extreme weather. Several materials used in PV modules such as junction box and frame adhesives, backsheets, and encapsulants can absorb moisture. In regions where temperatures often drop below freezing conditions, this moisture can freeze inside the module package. The expansion of moisture during this freezing process can be very detrimental to the module integrity. Ice crystals can cause failure of adhered interfaces resulting in delamination or other mechanical failure. Corrosion of the cell metallization and interconnect of the alloys can also be caused by these environmental changes [29].

Potential induced degradation

Potential Induced Degradation can arise when a voltage difference occurs between the panel and the earthing. During operation, because the modules are connected in series and the frames are connected together, cells experience a voltage bias relative to the module frame. In some cases, this generates a voltage which is partly discharged in the primary power circuit. The electric field between the solar cell and module frame causes sodium ions contained in the glass to diffuse either toward the cell or toward the frame that is away from the cell depending on the polarity of the voltage drop. This effect can damage cell properties and can result in a large reduction in

power output. Several system design decisions impact the voltage between the cells and frame such as system grounding configuration [30]. For safety, the solar panel is earth grounded.

Understanding the factors affecting the outdoor degradation and eventual failure of PV modules is crucial to the success of the Photovoltaic industry. A significant factor responsible for Photovoltaic module degradation is exposure to the Ultraviolet component of solar radiation.

Chapter 3

Modeling the Solar Cell

To define a solar cell model, it is necessary to represent the cell as an equivalent electric circuit. Numerous electric models have been developed to represent their non-linear behavior that results from the semi-conducting p-n junctions, which are at the base of their operation.

There are two primary circuit models of the solar cell

- One diode model (typically the general model).
- Two diodes model.

We will be discussing a Thévenin equivalent circuit for the one diode model which leads to a more direct analytical computation result:

3.1 Solar cell circuit model

A solar cell is traditionally represented by an equivalent circuit composed of a current source, an anti-parallel diode, a series resistance and a shunt resistance [8]. As shown in the diagram below.

A general circuit model [31] approximately representing a solar cell can be drawn as the following circuit.

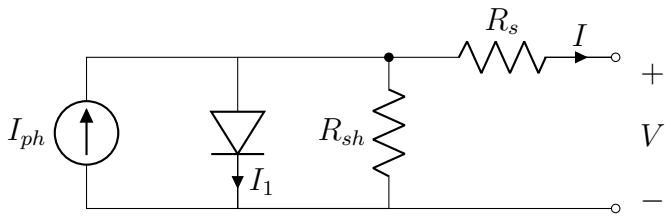

3.1.1 Characteristics of the solar cell

The main parameters that are used to characterize the performance of solar cells are the peak power (Pm), the short-circuit current (I_{sc}), the open circuit voltage (V_{oc}), and the fill factor (FF). These parameters are determined from the illuminated I-V characteristic curve and the efficiency can be derived from these parameters [8, 32–35]. The characteristics of the solar cell above can be summarized by the following equation for an ideal cell.

Using Kirchhoff's current law,

$$I = I_{ph} - I_d - I_{sh} \tag{3.1}$$

$$I = I_{ph} - I_d - \left(\frac{V + I \cdot R_s}{R_{sh}}\right) \tag{3.2}$$

the equation(3.2) can be further expressed by expanding the diode saturation current, I_d, to detail the intrinsic behavior of the solar cell operation [3, 31, 36, 37].

Here,

$$I_d = I_s \cdot \{exp(q(V + I \cdot R_s)/kT_C A) - 1\}\,. \tag{3.3}$$

In this circuit the diode acts as a current controlled current source. Hence, the circuit can then be re-written as

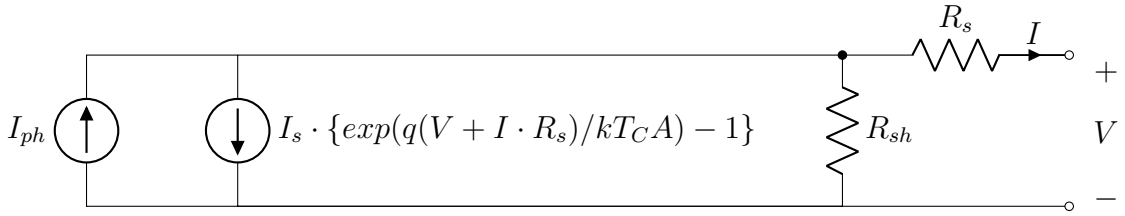

$$I = I_{ph} - I_s[exp\left(\frac{q \cdot (V + I \cdot R_s)}{kT_C A}\right) - 1] - \frac{V + I \cdot R_s}{R_{sh}} \tag{3.4}$$

where,

I = Output current

I_{ph} = Photo current

I_d = Diode saturation current

V = Voltage

R_s = Series resistance

R_{sh} = Shunt resistance

q = Electron charge

k = Boltzman constant

T_c = cell temperature

A = Ideality factor

3.1.2 The Photo-Current ($\mathbf{I}_{ph}$)

This is the current gotten from the intensity of the solar radiation. It is dependent on the temperature and the level of intensity. See figure 2.3. It is often referred to as

the illuminated current.

$$I_{ph} = I_{sc} + k_i \left(T - T_n\right) \frac{G}{G_n} \tag{3.5}$$

where,

G = Solar irradiance

G_n = Nominal solar irradiance at 1000W/m^2

T = Cell temperature

T_n = Nominal Temperature

k_i = Temp. coefficient of current.

I_{sc} = Short circuit current

Short Circuit Current

The short circuit current is obtained when the terminals of the cell are shorted yielding V=0. It grows linearly with the illumination intensity of the cell [38–40],

$$I_{sc} = I_{ph} - I_s[exp\left(\frac{I_{sc} \cdot R_s}{n \cdot \alpha}\right) - 1] - \frac{I_{sc} \cdot R_s}{R_{sh}} \tag{3.6}$$

For an ideal solar cell where by the mechanisms for resistive losses are small, the short-circuit current and the photo current are approximately identical. Therefore, the short-circuit current is the largest current which may be drawn from the solar cell. Taking the assumption that R_{sh} is much larger than R_s and that I_s is very small compared to I, the last two terms can be neglected, giving:

$$I_{sc} \approx I_{ph} \tag{3.7}$$

The short-circuit current depends on a number of factors such as the area of the cell, the number of photons, the (absorption and reflection) of the solar cell and the collection capacity of the solar cell.

3.1.3 Temperature

Variation in cell temperature occurs due to changes in the ambient temperature as well as changes in the intensity of solar radiation[8],the authors in [32] have it defined as

$$T = T_{amb} + \left(\frac{NOCT - 20^0C}{0.8}\right) \cdot G \tag{3.8}$$

where,

T_{amb} = Ambient temperature.

NOCT = Nominal operating cell temperature.

G = solar radiation.

Other methods for calculating the temperature were proposed and developed by the authors of [41], though the same results were gotten for the calculation of temperature. For this thesis, equation (3.8) was used.

Open Circuit Voltage

The open-circuit voltage is the voltage at which no current flows through the external circuit. It is the maximum voltage that a solar cell can deliver. The open-circuit voltage is obtained when the current flowing through the cell is zero. It depends on the energy barrier and shunt resistance. It decreases with an increase in temperature and varies little with light intensity [8, 31, 33, 36, 42]. For $I = 0$,

$$0 = I_{ph} - I_s[exp\left(\frac{q \cdot V_{oc}}{kT_C A}\right) - 1] - \frac{V_{oc}}{R_{sh}} \tag{3.9}$$

3.1.4 Diode Saturation Current

The leakage current which passes through the diode varies with the cell temperature which is given in [40]

$$I_s = I_{rs}\left[\frac{T}{T_n}\right]^3 exp\left[\frac{q \cdot E_{go}}{n \cdot k}\left(\frac{1}{T} - \frac{1}{T_n}\right)\right] \tag{3.10}$$

Similarly, at S.T.C we get the reverse saturation current, I_{rs} [31].$From$ [40]$wecanwrite$

$$I_{rs} =$$

where,

q = electron charge = 1.6 x $10^{-}19$C

N_s = number of connected cells

K = Boltzman's constant = 1.3805 x $10^{-}23$J/K

3.1.5 Maximum Power

Power delivered by the PV cell is the product of voltage (V) and current (I). At both open and short circuit conditions the power delivered is zero. The I-V characteristics of a solar cell maximum power will occur at the bend point of the characteristic curve. See figure 3.5. The maximum amount of current that a PV cell can deliver is the short circuit current. Given the linearity of current in the voltage range from zero to the maximum power point voltage, the use of the short circuit current for cable and system dimensioning is reasonable.

Since the cell current is dependent on the amount of irradiance falling on the PV cell and the cell's temperature, the maximum power would shift depending on the variations. The irradiance decreasing not only affects the amount of power, but the peak power point would move to the left. While the temperature of the cell increases, the power output lowers and the maximum power point again shifts to the left. Due to these dependencies recent inverters have mechanisms called "maximum power point tracking" that tracks this movement and possibly delivers maximum power.

Fill Factor (FF)

The conversion efficiency is calculated as the ratio between the maximal generated power and the incident power, See figure 3.1. The fill factor would slightly increase or decrease depending on the intensity of the irradiance and the influence of parasitic resistance [35, 43].

$$FF = \frac{I_{mp} \cdot V_{mp}}{I_{sc} \cdot V_{oc}} \tag{3.12}$$

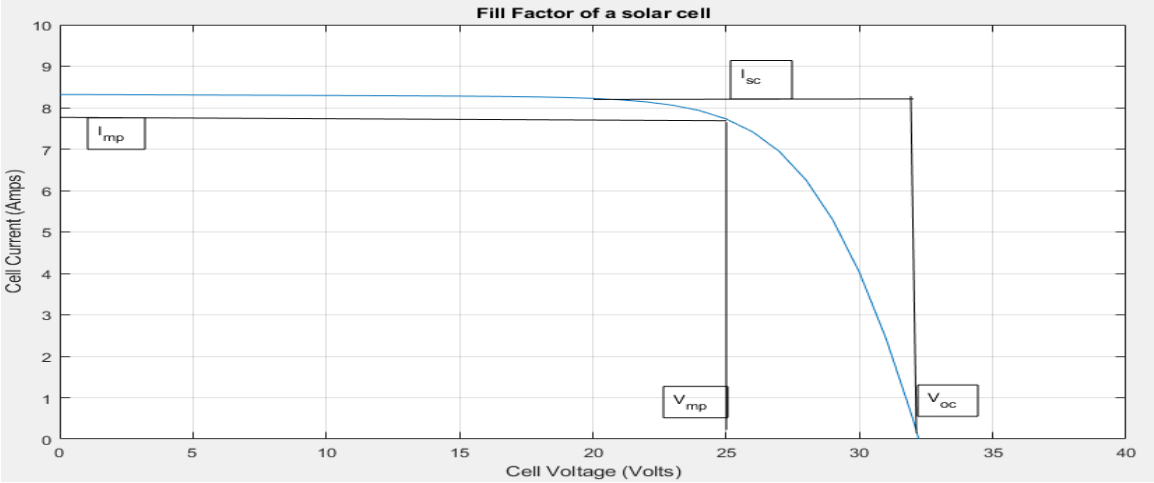

Figure 3.1: Fill factor of the solar model

Efficiency

Efficiency is defined as the ratio of maximum electrical power output to the radiation power input(P_{in}) of the cell and it is expressed in percentage. Simply put, it measures the amount of solar energy falling on the Photovoltaic cell which is converted to electrical energy. It is assumed that the radiation power measured on the earth is about 1000W/m^2.

Hence, if the exposed surface area of the cell is 'S' then total radiation power on the cell will be (1000 S) watts. Therefore, the efficiency of a solar cell may be expressed as

$$\eta = \frac{I_{mp} \cdot V_{mp}}{P_{in} \cdot S} \tag{3.13}$$

The efficiency of a module can usually be found on the data sheet from the manufacturer. this characteristic is important cause the efficiency can be used to sort modules into different levels of productivity and cost. That is, more efficient cells would have a greater electrical output and hence higher cost. The efficiency is also

affected over a long time (>20 years) in most cases by degradation mechanisms. Growing research and development in solar technologies are now starting to exploit the limits of semiconductor devices.

3.1.6 Ideality Factor

The ideality factor accounts for the different mechanisms responsible for moving carriers across the junction. The parameter $n \approx 1$ if the transport process is purely diffusion and $n \approx 2$ if it is primarily recombination in the depletion region. In [44] the authors suggest an $n \approx 1.3$ for silicon. The ideality factor, n, is assumed to be related only to the material of the solar cell and be independent of temperature and solar irradiation[32].

The ideality factor can be calculated, if the other parameter's values such as the photocurrent, diode saturation current, series resistance, and shunt resistance are known, along with the operational data provided by the manufacturer. This method was proposed in [45] where Lambert W-Functions were used to solve for the ideality factor. The ideality factor as a parameter is described to define the extent in which the solar cell behaves as an ideal diode, therefore the factor itself will not change when the cell is operating[34, 46].

For ideality factor,the parameters can be obtained in a general forms with respect to standard test conditions data as

$$n = \frac{q \cdot v_d}{KT\,(InI - InI_s)} \tag{3.14}$$

3.1.7 Resistance

The parallel leakage resistance or shunt resistance,R_{sh}, and series resistance,R_s, are the last two parameters . As an approximation[8],

$$R_{sh} \geq \frac{10 \cdot V_{oc}}{I_{sc}}$$

$$R_s \leq \frac{0.1 \cdot V_{oc}}{I_{sc}}$$

where, V_{oc} and I_{sc} are open circuit voltage and short circuit current respectively.

Some research papers such as the five parameter method discussed in [41] state the assumption that the series resistance is independent of temperature and irradiation at both operating conditions and Standard Reference Condition, while also relating the relationship of the shunt resistance to irradiation at operating conditions and Standard Reference Condition.

3.2 Simulated Results

The I-V curve of the solar cell can be simulated with software such as Matlab/ Simulink as shown below. Using the information extracted from the data sheet of the RNG -160D-SS panel [10, 47], an electrical simulink model of a solar cell can be constructed as follows.

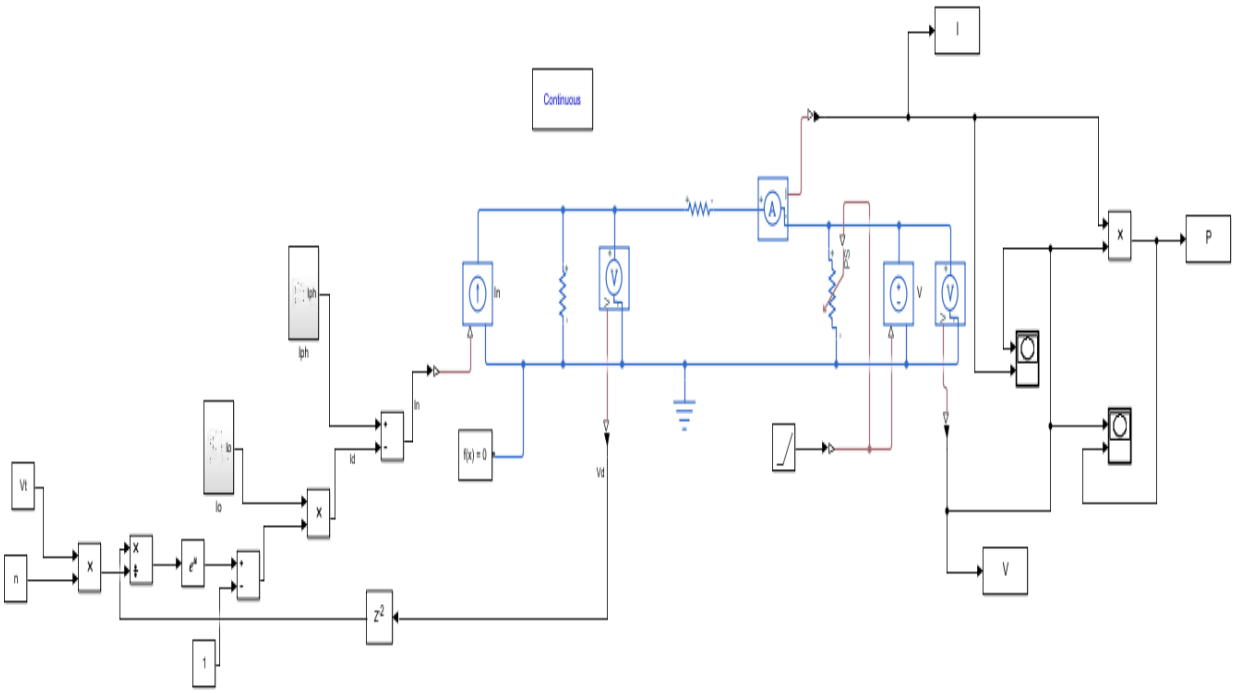

Figure 3.2: Electrical simulink model

A mathematical model can be implemented as follows.

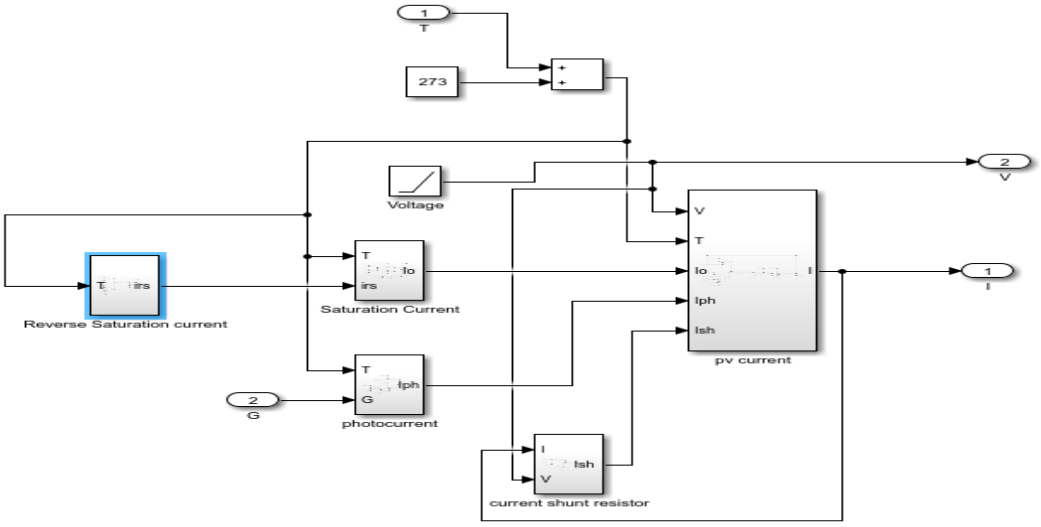

Figure 3.3: Mathematical simulink model

Although similar results of the I-V curve can be derived from either model, the only major difference between the two models is the composition of the models themselves. One is solely built on characteristic equations,the various equations are shown in Appendix C i.e. the mathematical based model. The other tries to inculcate a more circuit defined approach. The resulting waveforms and curves from the model shown above are the current - voltage characteristic curve and the power - voltage curve of the solar cell.

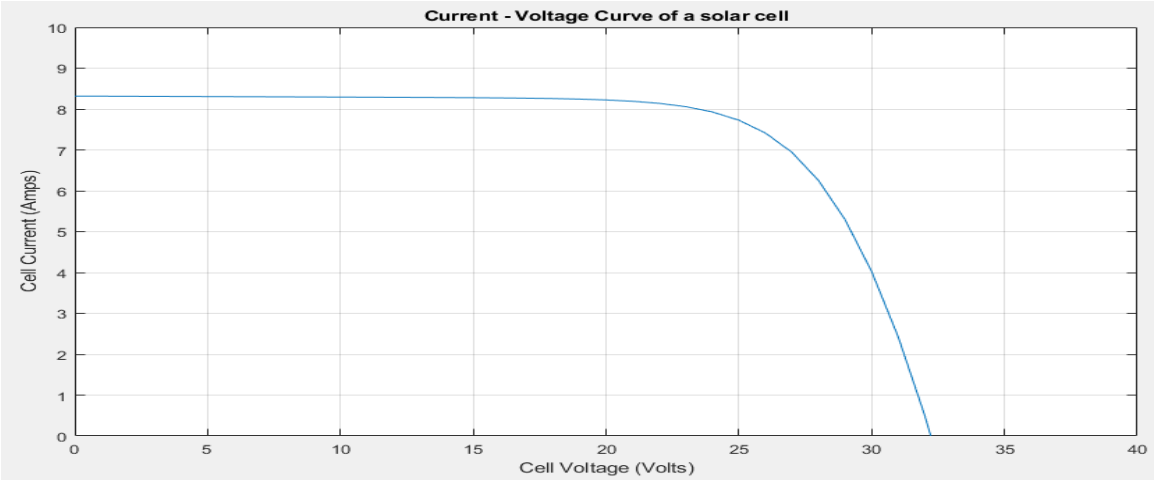

Figure 3.4: I-V curve of the solar cell model

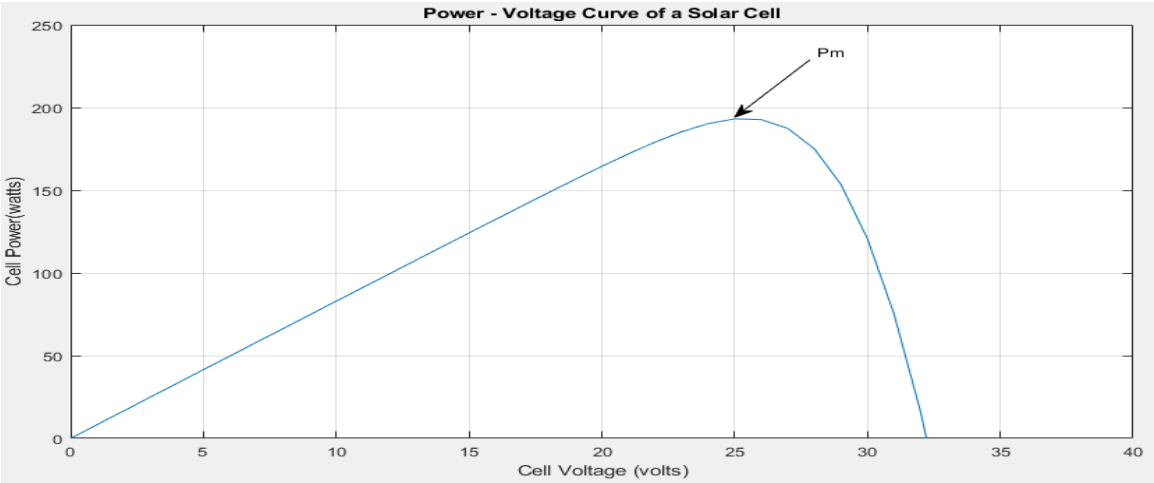

Figure 3.5: P-V curve of the solar cell model

In photovoltaics, the maximum current of a PV module is obtained at a resistance, $R = 0$, in the circuit. This can be brought about by bridging of the Positive and Negative terminals. Similarly, the maximum voltage occurs when there is a break in the circuit. Under this condition, the resistance is infinitely high and the current, $I = 0$, since the circuit is incomplete. From the plots above, figure 3.4 and 3.5, we can see the two extremes in load resistance and the range of conditions in between them. On the knee of the I-V curve we get the maximum power of the cell. The

power available from a photovoltaic cell at any point along the curve is a the product of Current and Voltage. Also of note the power output, $P = 0$, occurs at the short circuit current point and the open circuit voltage point.

3.2.1 Effects of Irradiance

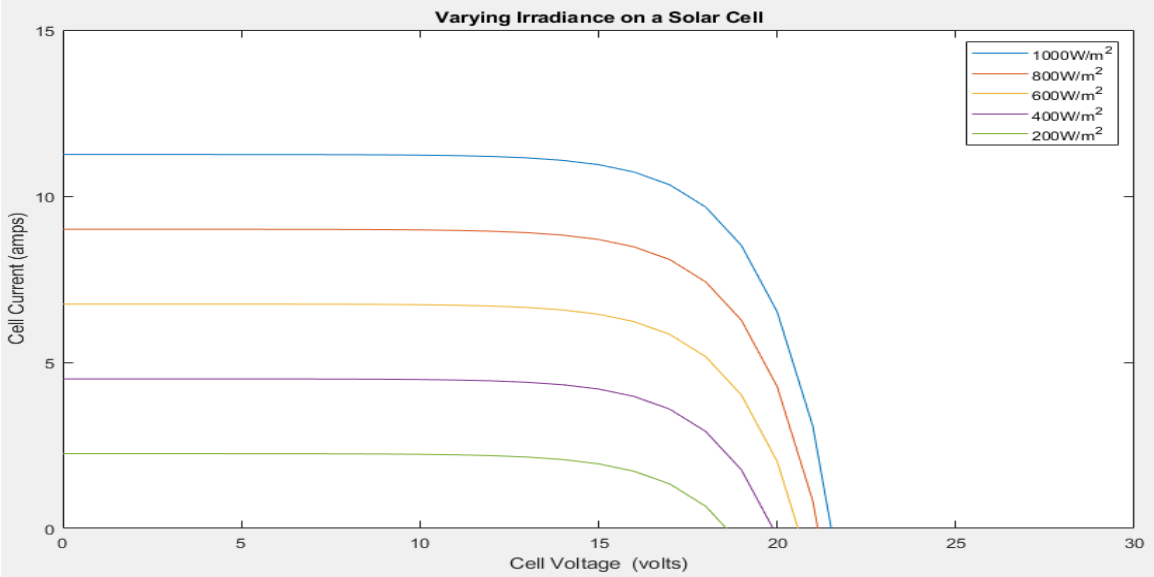

Figure 3.6: I-V curve for varying solar irradiance

The irradiance from the sun varies from 200 - 1000W/m^2 with an increment of 200W/m^2 while keeping other parameters constant. the increase in irradiance reflects on the current as it increases linearly as shown in fig 3.6.

3.2.2 Effects of Temperature

Temperature increases on the solar cell leads to a linear decrease in the open circuit voltage, hence a drop in the cell efficiency.

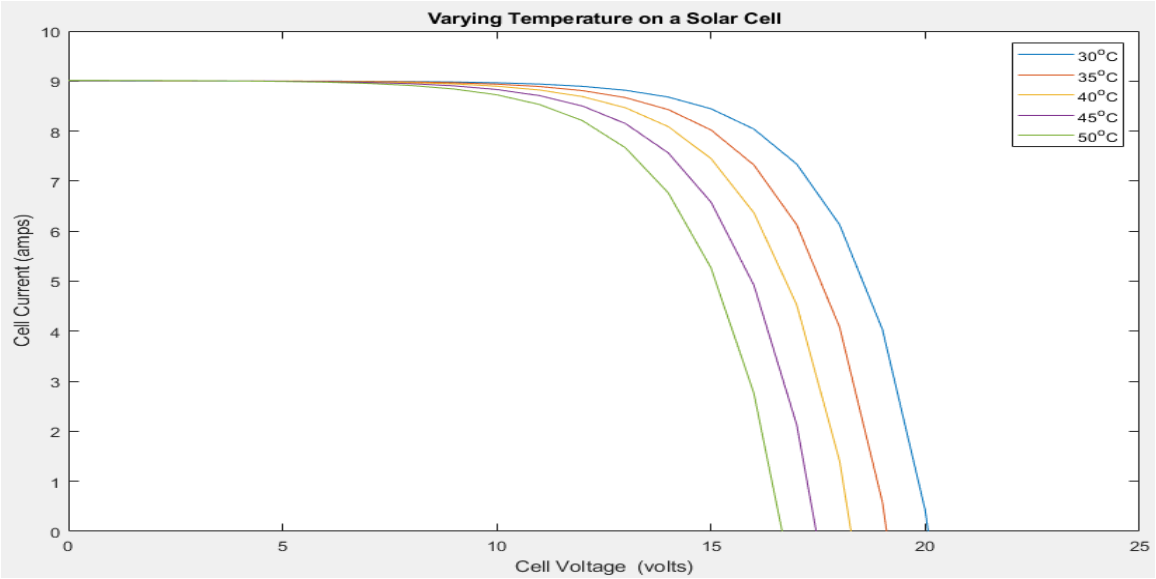

Figure 3.7: I-V curve for varying temperature

3.2.3 Effects of Resistances

The operating condition dependence of the series resistance and the shunt resistance completes the investigation into the model. The series resistance impacts the shape of the current - voltage curve near the maximum power point. This effect can be seen in figure 3.8 in which the current–voltage curves for the single-crystalline cell at STC conditions have been plotted for varying series resistance values derived from the five parameter method.

Although the effect on the I–V curve is small, but with an increase possibly due to degradation mechanisms, its effects would gradually increase. Nevertheless,

methods of adjusting series resistance as a function of operating conditions have been investigated[41]. In this thesis, we would assume that the series resistance varies with influence of internal and external factors.

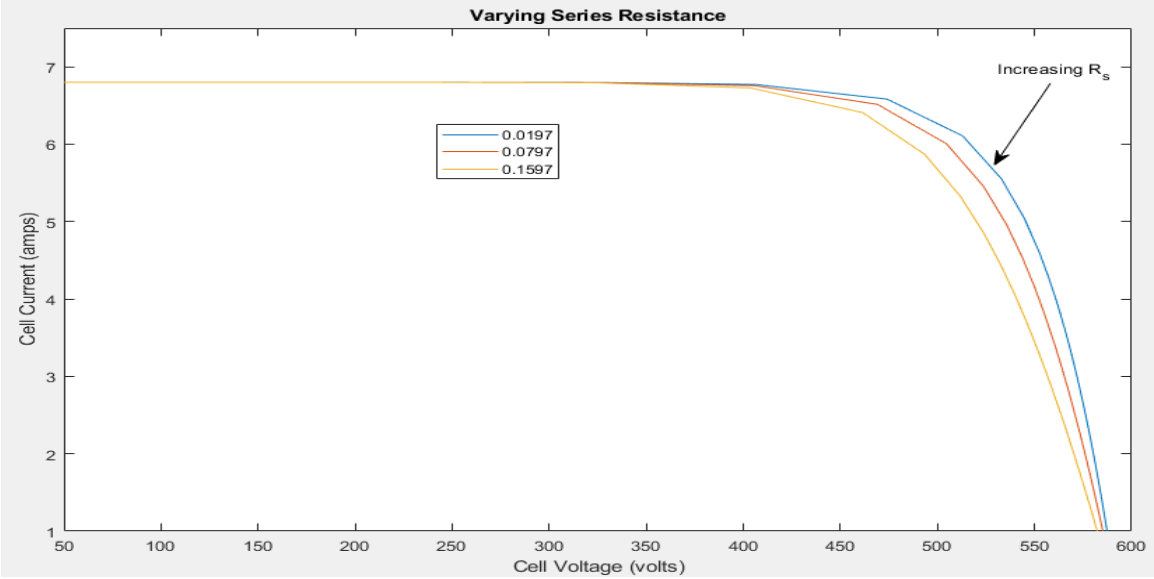

Figure 3.8: I-V curve for varying Series resistance

The shunt resistance can be measured using the slope of the I–V curve at the short circuit condition. With a decrease in the shunt resistance the slope tilts downwards. This would indicate a low shunt resistance, in such a situation the solar cells would potentially lose power by providing an alternate current path for the light-generated current. Such diversions would reduce the amount of current flowing through the solar cell junction and reduces the voltage across the solar cell, hence reducing cell efficiency.

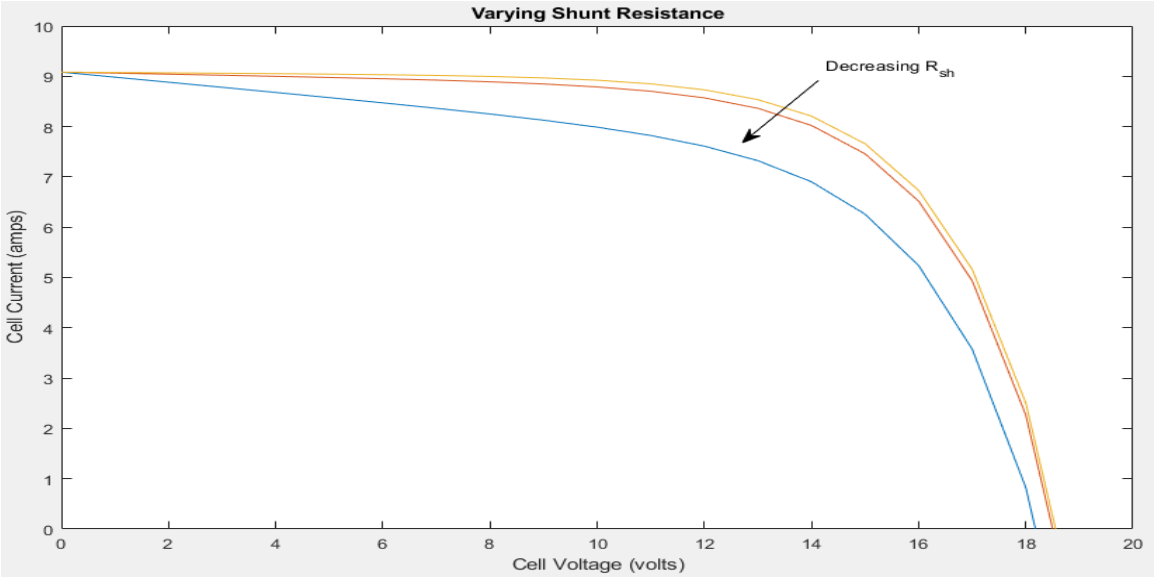

Figure 3.9: I-V curve for varying shunt resistance

Some of the model parameters are empirically based. Others can be determined through testing but have dependencies associated with various operating conditions such as temperature. See figures (3.4 - 3.9). Two parameters in particular, R_S and R_{SH}, i.e. the series and shunt equivalent resistances, can vary under different operating conditions and may experience variation over time. These variations are important to characterize particularly given the relatively long operating cycle of a typical solar cell in use within an encapsulated panel. Many contemporary panel manufacturers claim as much as twenty-five (25) years expected operation with limited degradation[9, 10].

3.3 Determination of parameters

Most parameters of the solar cell can be determined by examining the manufacturer's data sheet. Parameters that are mostly needed for describing the solar cell electrical performance, specifically the the open-circuit voltage V_{oc} and the short-circuit current

I_{sc} [34, 35, 38–40]. Operational data on the cell or PV module such as the open-circuit voltage V_{oc} , the short-circuit current I_{sc} , the maximum power point current I_{mp} , voltage maximum point V_{mp} and the temperature coefficients of the open-circuit voltage and the short-circuit current (T_β and T_α) respectively are typically shown on the data sheet[9, 10].

However, some data sheets do not have all the parameters shown as such the operational data is used to estimate for the other parameters R_s, R_p, I_s, n using numerical analysis. There are several methods proposed over the years to determine and estimate these parameters such as Lambert function and Newton Rapson method among others. [33–35, 38, 39, 45]. Most of the parameters that can be extracted with respect to Standard Test Conditions.

For the shunt resistance, the inverse of the slope of the I-V curve see figure 3.9 at short circuit current gives

$$R_{sh} \approx \frac{-dV}{dI} \tag{3.15}$$

The series resistance is taken as a lumped parameter to include all series resistances of the solar cells such as cables,joints, etc. enabling easier computations and access to the effect of series resistances in the PV module. However for the production of a PV module various materials and cells with various I-V characteristics are used. So a high series resistance may be caused by the addition of series resistances in the module or caused by a mismatch of the individual cell characteristics. For the series resistance at open circuit voltage,

$$R_s \approx \frac{dV}{dI} \tag{3.16}$$

Chapter 4

Methodology using the Thévenin equivalent circuit

4.1 Thévenin equivalent circuit

Here we derive a Thévenin equivalent circuit from the perspective of the output terminals. For computational simplicity an intermediate variable, α, is introduced. Therefore, $\alpha = \frac{kT_C A}{q}$.

First, to determine the Thévenin equivalent voltage, V_{TH}, we note that at the open circuit terminals the current is $I = 0$. Then,

$$\left\{ I_{ph} - I_S \cdot \left\{ exp\left(\frac{V_{TH}}{\alpha}\right) - 1 \right\} \right\} \cdot R_{sh} = V_{TH}$$

We note that for small β, $e^{\beta} \simeq 1 + \beta$. This small exponent approximation is appropriate in our case given V_{TH} is small. This occurs under low solar irradiance conditions. Therefore,

$$exp\left(\frac{V_{TH}}{\alpha}\right) - 1 \simeq 1 + \frac{V_{TH}}{\alpha} - 1 = \frac{V_{TH}}{\alpha}$$

Now,

$$\begin{aligned} I_{PH} \cdot R_{SH} = &\quad V_{TH} + I_S \cdot R_{SH} \cdot \tfrac{V_{TH}}{\alpha} \\ I_{PH} \cdot R_{SH} = &\quad V_{TH} \cdot \left(1 + \tfrac{I_S \cdot R_{SH}}{\alpha}\right) \end{aligned}$$

$$V_{TH} = \frac{I_{PH} \cdot R_{SH}}{\left(1 + \frac{I_S \cdot R_{SH}}{\alpha}\right)} \tag{4.1}$$

Once the equivalent voltage is obtained, we determine the Thévenin equivalent resistance, R_{TH}. Since the equivalent circuit model has a dependent source, we disable all independent sources and inject a known $1A$ source between the output terminals and again seek voltage, V, measured across the terminals.

Then, $R_{TH} = \frac{V}{1A} = V$. Hence, The circuit can be written as,

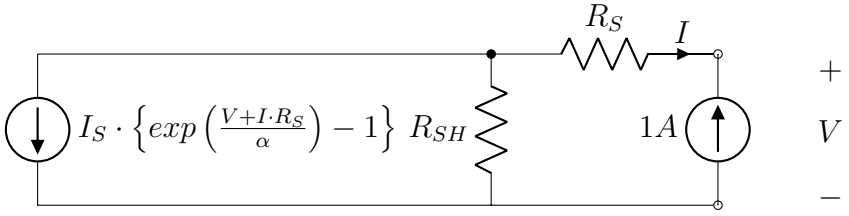

where $I = -1$. Using source conversion we have

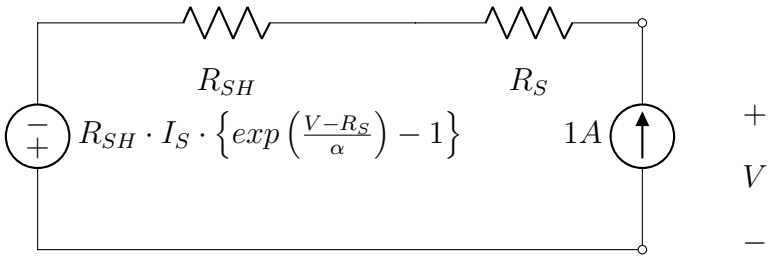

Now using Kirchoff's Voltage Law we have

$$V = (R_S + R_{SH}) - R_{SH} \cdot I_S \cdot \left\{ exp\left(\frac{V - R_S}{\alpha}\right) - 1 \right\}. \tag{4.2}$$

For $V > R_S$, taking R_S to be small, we use the small exponent approximation again yielding

$$exp\left(\frac{V - R_S}{\alpha}\right) - 1 \simeq \left(\frac{V - R_S}{\alpha}\right)$$

Therefore,

$$V \simeq R_S + R_{SH} - R_{SH} \cdot I_S \cdot \left(\frac{V - R_S}{\alpha}\right)$$

Simplifying yields,

$$V \simeq R_S + R_{SH} - \left(\frac{R_{SH} \cdot I_S}{\alpha}\right) \cdot V + \left(\frac{R_S \cdot R_{SH} \cdot I_S}{\alpha}\right)$$

$$V \simeq \frac{R_S + R_{SH} + \left(\frac{R_S \cdot R_{SH} \cdot I_S}{\alpha}\right)}{1 + \left(\frac{R_{SH} \cdot I_S}{\alpha}\right)}$$

$$\Rightarrow R_{TH} \simeq \frac{R_S + R_{SH} + \left(\frac{R_S \cdot R_{SH} \cdot I_S}{\alpha}\right)}{1 + \left(\frac{R_{SH} \cdot I_S}{\alpha}\right)} \tag{4.3}$$

Since the current going through the R_{SH}, that is I_{SH}, is much larger than I_s. Then $I_{SH} >> I_S$ and I_{SH} is assumed low under low solar irradiance conditions[1] and $I_S \simeq 0$. Then we can simplify the Thévenin equivalent voltage and resistance as follows

$$V_{TH} \simeq I_{PH} \cdot R_{SH}$$

$$R_{TH} = V \simeq R_S + R_{SH}.$$

This oversimplification assumes the R_S to be approximately zero, therefore $R_{TH} \simeq R_{SH}$. Disregarding the simplifications where R_S may vary due to illumination intensity[1], the resulting Thévenin equivalent circuit becomes

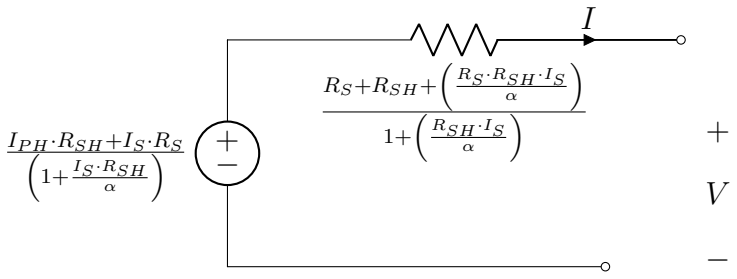

4.2 Test Methodology

The Thévenin equivalent circuit represents a solar cell given that an appropriate parameter value is used for α. Then an in situ test load can be used to derive R_S and R_{SH}. The procedure requires an adjustable solid state resistive load, a two position switch or relay, a capacitor, and voltage measurement across the output of the solar cell under low solar irradiance conditions. The procedure is as follows:

1. Measure the open circuit voltage of the cell, V_{oc}. This generates the following

constraint,

$$V_{oc} = \frac{I_{PH} \cdot R_{SH} + I_S \cdot R_S}{\left(1 + \frac{I_S \cdot R_{SH}}{\alpha}\right)} \tag{4.4}$$

In addition, from equation (4.1) we have

$$\frac{V_{oc}}{R_{SH}} = I_{PH} - I_d \tag{4.5}$$

2. Now connect a capacitor of known value creating an RC charging circuit using the relay. Measure the RC time constant τ_1 via voltage measurements across the capacitor. At the end of the charge cycle, $I \simeq 0$ and $V \simeq V_{oc}$.

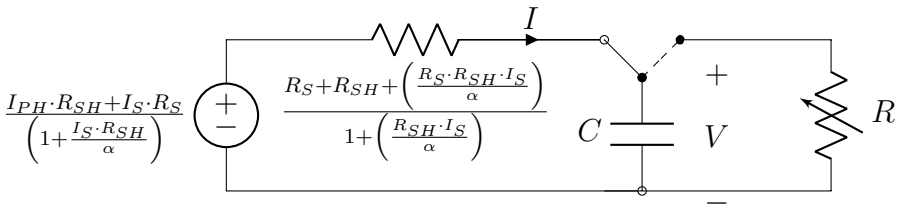

We can determine the charge and current equations by considering KVL,

$$R_S + \frac{R_{SH} + \alpha}{(\alpha + R_{SH} \cdot I_S)} = V_{TH}[1 - e^{\frac{-\tau}{RC}}]$$
$$\frac{1}{V_{TH}}\left(R_S + \frac{R_{SH} + \alpha}{(\alpha + R_{SH} \cdot I_S)}\right) - 1 = -e^{\frac{-\tau}{RC}}$$

Now applying a natural log to both sides and rearranging the equation yields

$$\tau = R \cdot C \cdot ln[\frac{1}{V_{TH}}\left(R_S + \frac{R_{SH} + \alpha}{(\alpha + R_{SH} \cdot I_S)}\right)] \tag{4.6}$$

3. Then switch the relay so that the capacitor discharges to the variable resistor. Measure the time constant, τ_2, and compare to τ_1 determined in the previous step. If $\tau_1 > \tau_2$, adjust R higher. If $\tau_2 > \tau_1$ adjust R lower. Repeat this step until $\tau_2 \simeq \tau_1$.

$$R = \frac{R_S + R_{SH} + \left(\frac{R_S \cdot R_{SH} \cdot I_S}{\alpha}\right)}{1 + \left(\frac{R_{SH} \cdot I_S}{\alpha}\right)} \tag{4.7}$$

It is reasonable to assume $I_1 \simeq 0$ under these test conditions and that $I_S \propto I_{SH}$ such that $I_S = \beta \cdot I_{SH}$ with known β from empirical test data. Therefore, equations (4.4), (4.5), and (4.7) can be used to derive R_S and R_{SH}. This procedure can be utilized as a periodic test to measure drift of the lumped resistance parameters.

$$V_{oc} = V_{oc} + I_S \cdot R_S\left(1 + \frac{I_S \cdot R_{SH}}{\alpha}\right)$$

$$V_{oc} \cdot \left(1 + \frac{I_S \cdot R_{SH}}{\alpha}\right) = I_S \cdot R_S$$

$$V_{oc} = \frac{R_S \cdot \alpha}{R_{SH}} \tag{4.8}$$

This system is under constrained with three unknown variables. Many possible models suggest a strong dependency of temperature on I_S effects due to varying irradiance levels and temperatures. Therefore under varying temperatures we assume a change in I_S given changes in temperature where irradiance levels are held fixed would yield a change in the measured R,

$$R(T) = \frac{R_S + R_{SH} + \left(\frac{R_S \cdot R_{SH} \cdot I_S(T)}{\alpha(T)}\right)}{1 + R_{SH} \cdot I_S(T)} \tag{4.9}$$

If this change is approximately linear with respect to temperature, we have $I_S(T) = m \cdot T$.

Therefore,

$$R(T_1) = \frac{R_S + R_{SH} + \left(\frac{R_S \cdot R_{SH} \cdot m \cdot T_1)}{\alpha(T_1)}\right)}{1 + R_{SH} \cdot m \cdot T_1} \tag{4.10}$$

$$R(T_2) = \frac{R_S + R_{SH} + \left(\frac{R_S \cdot R_{SH} \cdot m \cdot T_2)}{\alpha(T_2)}\right)}{1 + R_{SH} \cdot m \cdot T_2} \tag{4.11}$$

It remains to solve for R_S, R_{SH}, and m given equations (4.8), (4.10), and (4.11). Substituting into equations (4.10) and (4.11) yields

$$R(T_1) = \frac{R_S + \frac{R_S \cdot \alpha(T_1)}{V_{oc}} + \frac{R_S^2 \cdot m \cdot T_1}{V_{oc}}}{1 + \left(\frac{R_S \cdot \alpha(T_1) \cdot m \cdot T_1}{V_{oc}}\right)} \tag{4.12}$$

$$R(T_2) = \frac{R_S + \frac{R_S \cdot \alpha(T_2)}{V_{oc}} + \frac{R_S^2 \cdot m \cdot T_2}{V_{oc}}}{1 + \left(\frac{R_S \cdot \alpha(T_2) \cdot m \cdot T_2}{V_{oc}}\right)} \tag{4.13}$$

Now given

$$\beta_1 = R(T_1)$$

$$\beta_2 = \frac{R(T_1) \cdot \alpha(T_1) \cdot T_1}{V_{oc}}$$

$$\beta_3 = \frac{\alpha(T_1)}{V_{oc}}$$

$$\beta_4 = \frac{T_1}{V_{oc}}$$

We can write the following equations for m

$$\beta_1 + \beta_2 \cdot R_S \cdot m = R_S + \beta_3 \cdot R_S + \beta_4 \cdot R_S^2 \cdot m$$

$$m \cdot \left(\beta_4 \cdot R_S^2 - \beta_2 \cdot R_S\right) = \beta_1 - R_s \cdot (1 + \beta_3)$$

$$m = \frac{\beta_1 - R_s \cdot (1 + \beta_3)}{\beta_4 \cdot R_S^2 - \beta_2 \cdot R_S} \tag{4.14}$$

Now substitute m in equation (4.11) to solve for R_S. Then R_{SH} can be found by rewriting equation (4.8).

$$R_{SH} = \frac{R_S \cdot \alpha}{V_o c}$$

This procedure can be utilized as a periodic test to measure drift of the lumped resistance parameters.

4.2.1 Simulated Results

The Thévenin equivalent circuit model was built in Simulink utilizing the mathematical equations from above. The model is shown in the figure below.

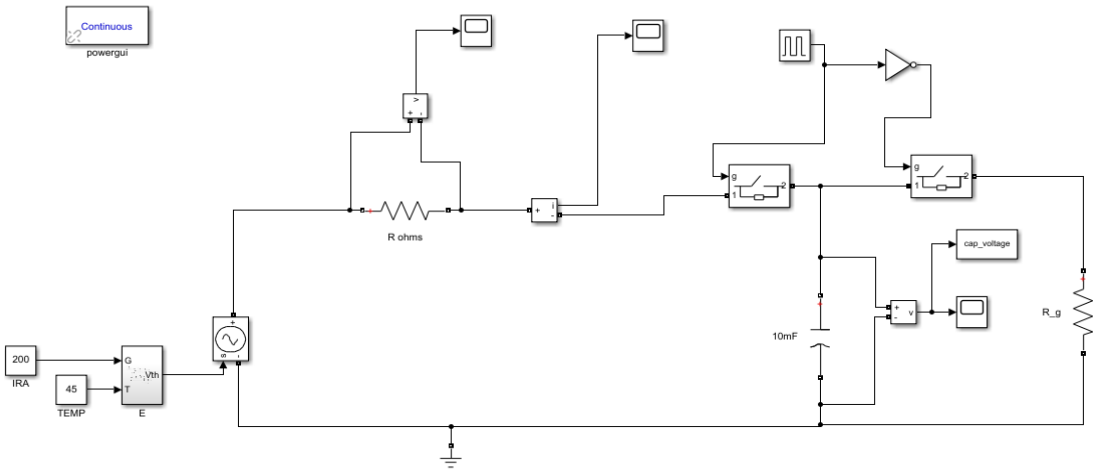

Figure 4.1: Thévenin equivalent circuit model

The resulting waveform shows the capacitor voltage under conditions where $\tau_1 > \tau_2$. The resistance, R, is adjusted higher and when $\tau_2 > \tau_1$ the resistance R is adjusted lower. As the time constants approach each other the capacitor voltage curve oscillates about an equilibrium. This is evident from the ripple waveform shown in figure 4.2. The time taken for this varies with the increase or decrease of the lumped resistance which is also affected by the light intensity and temperature. Hence the lumped resistance of the solar cell can be derived/estimated.

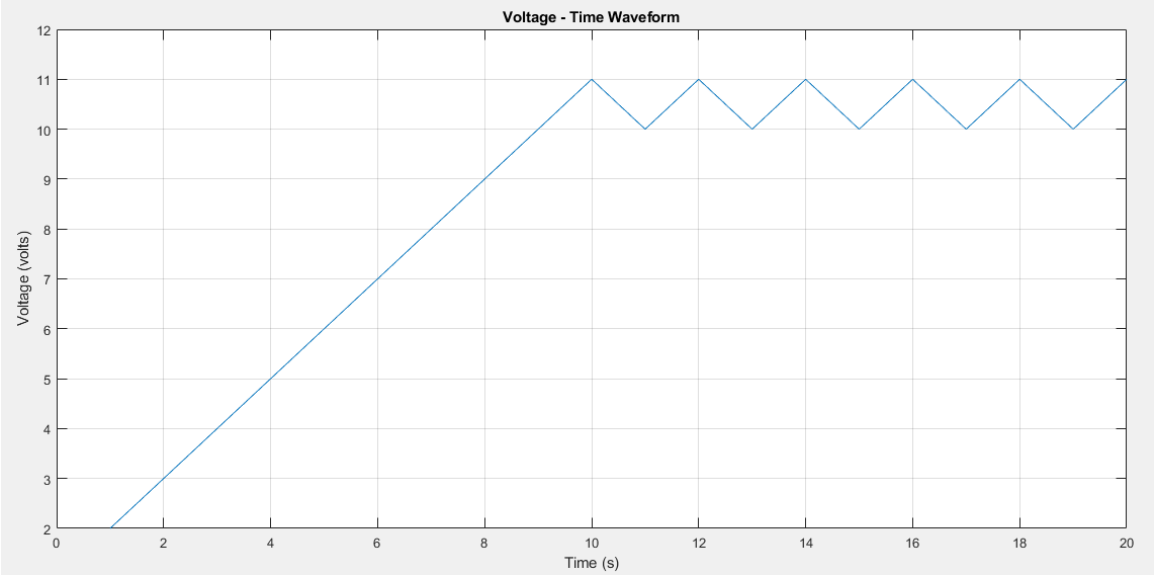

Figure 4.2: Capacitor voltage - time waveform

In comparison, the solar cell substituted into the proposed Thévenin equivalent circuit simulink model as a source to drive the VCS shows a similar wave form pattern. Whereby, as the time constants approach each other, the capacitor voltage curve oscillates about an equilibrium as shown in figure 4.3. Therefore, using Thévenin theory, we were able to derive the single voltage source and lump resistance.

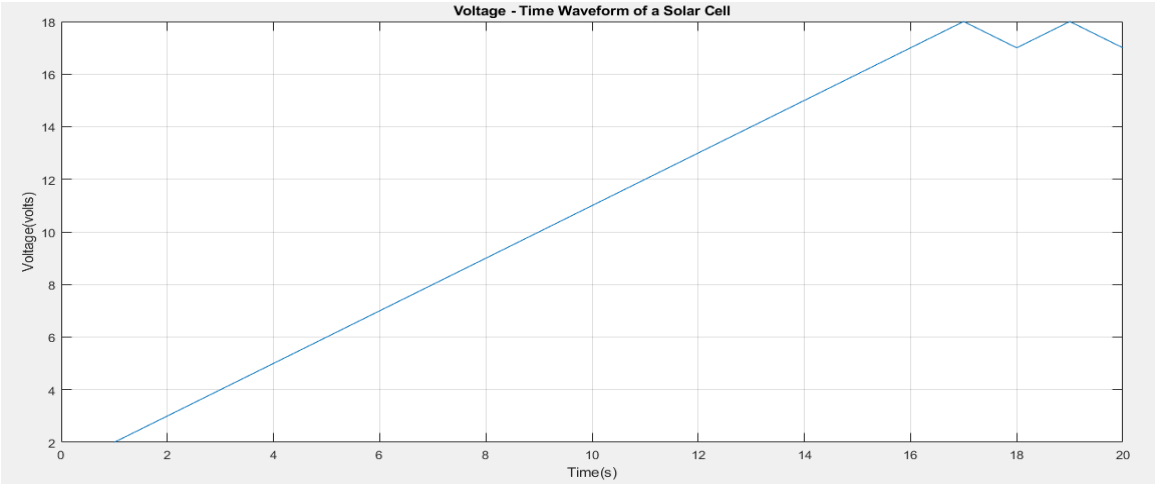

Figure 4.3: Capacitor voltage - time waveform solar cell

Conclusion

The model presented in this thesis uses only data provided by the manufacturer with semi-empirical equations to predict the cell I–V curve for any operating condition. The model requires a one-time calculation of the parameters at reference conditions. The values are then used within the model to run the simulation, making it possible to predict the lumped resistance. The modeling results derived in this thesis made use of a low irradiance assumption to generate simplifying approximations. For this, certain low light periods during the day would provide the necessary environment to justify the model approximations. Further extensions to these results by relaxing the low irradiance assumption is desired to allow for more flexible test conditions. With improvements these results aim to measure the lumped resistance os solar cells at various power thresholds and could be used to monitor degradation and improve solar cell estimated life cycle characterization.

Bibliography

[1] K. C. Fong, K. R. Mclntosh, and A. W.Blakers, "Accurate series resistance measurement of solar cells," *Progress in Photovoltaics: Research and Applications*, 2011.

[2] D.Pysch, A.Mette, and S.W.Glunz, "A review and comparison of diferent methods to determine the series resistance of solar cells," *Solar Energy Materials and Solar cell*, vol. 91, pp. 1698–1706, 2007.

[3] M. S. Benghanem and S. N. Alamri, "Modelling of photovoltaic module and experimental determinaton of serial resistance," *Jof Taibah University for Science*, 2009.

[4] D. Chapin, C. Fuller, and G. Pearson, "A new silicon pn junction photocell for converting solar cell into electrical power," *journal of Applied Physics*, vol. 25, 1954.

[5] A. El-Ghonemy, "Photovoltaic solar energy: Review," *International Journal of Scientific & Research*, vol. 3, November 2012.

[6] "Renewable energy technologies: cost analysis series," 2012.

[7] L. castaner and santiago silvestre, *Modelling Photovoltaic Systems Using PSpice*, ch. 2, pp. 19–39. John Wiley Sons,Ltd, 2006.

[8] G. M. Masters, *Renewable and Efficient Electric Power Systems*. Wiley, 2013.

[9] I. First Solar, "First solar series 4™ datasheet." `http://www.firstsolar.com/-/media/First-Solar/Technical-Documents/Series-4-Datasheets/Series-4V3-Module-Datasheet.ashx`, Sep 2018.

[10] Renogy, "Rng-160d-ss datasheet." `https://www.renogy.com/content/files/Specifications/RNG-160D-SS%20spec.pdf`. accessed on march 2019.

[11] B. V. Chikate and Y. Sadawarte, "The factors affecting the performance of solar cell," *International Journal of Compter Applications*, 2015.

[12] T. Welch, "Photovoltaics for buildings." `https://www.cibsejournal.com/cpd/modules/2010-01/`, 2010.

[13] F. Peacock, "Solar panels." `https://www.solarquotes.com.au/panels/photovoltaic/monocrystalline-vs-polycrystalline/`, 2019.

[14] A. Hossam-Eldin, M. Refaey, and A. Farghly, "A review on photovoltaic solar energy technology and its efficiency," 12 2015.

[15] "Thin silicon string ribbon," *Solar Energy Materials and Solar Cells*, vol. 48, no. 1, pp. 179 – 186, 1997.

[16] M. A. Green, Y. Hishikawa, E. D. Dunlop, D. H. Levi, J. Hohl-Ebinger, and A. W. Ho-Baillie, "Solar cell efficiency tables (version 51)," *Progress in Photovoltaics: Research and Applications*, vol. 26, no. 1, pp. 3–12, 2018.

[17] "Economical and highly efficient non-metal counter electrode materials for stable dye-sensitized solar cells," in *Dye-Sensitized Solar Cells* (M. Soroush and K. K. Lau, eds.), pp. 397 – 435, Academic Press, 2019.

[18] M. Hösel, D. Angmo, and F. Krebs, "Organic solar cells (oscs)," in *Handbook of Organic Materials for Optical and (Opto)electronic Devices* (O. Ostroverkhova, ed.), Woodhead Publishing Series in Electronic and Optical Materials, pp. 473 – 507, Woodhead Publishing, 2013.

[19] W. Hurter, H. Plessis, and N. Rensburg, "Simplified encapsulation of solar cells using glass fibre reinforced polymers," in *The Conference Record of the Twenty-Second IEEE Photovoltaic Specialists Conference - 1991*, pp. 1–5, 09 2013.

[20] K. Agroui, M. Jaunich, and A. H. Arab, "Analysis techniques of polymeric encapsulant materials for photovoltaic modules: Situation and perspectives," *Energy Procedia*, vol. 93, pp. 203 – 210, 2016. Africa-EU Symposium on Renewable Energy Research and Innovation.

[21] H. Wirth, K.-A. Weiß, and C. Wiesmeier, *Photovoltaic Modules: Technology and Reliability*. Walter de Gruyter GmbH & Co, 2016.

[22] C. Honsberg and S. Bowden, "Modules and array." https://www.pveducation.org/pvcdrom/modules-and-arrays/degradation-and-failure-modes, 2019.

[23] M. Köntges, S. Kurtz, K. A. Berger, and K. K. et al, "Performance and reliability of photovoltaic systems," final, International Energy Agency Photovoltaic Power Systems Programme, March 2014.

[24] D. Jordan and S. Kurtz, "Photovoltaic degradation rates—an analytical review," *Progress in Photovoltaics: Research and Applications*, vol. 21, 01 2013.

[25] M. Oliveira, A. Cardoso, M. Viana, and V. Lins, "The causes and effects of degradation of encapsulant ethylene vinyl acetate copolymer (eva) in crystalline silicon

photovoltaic modules: A review," *Renewable and Sustainable Energy Reviews*, 07 2017.

[26] C. Radue and E. van Dyk, "A comparison of degradation in three amorphous silicon pv module technologies," *Solar Energy Materials and Solar Cells*, vol. 94, no. 3, pp. 617 – 622, 2010.

[27] H. J. Wenger, J. Schaefer, A. Rosenthal, B. Hammond, and L. Schlueter, "Decline of the carrisa plains pv power plant: the impact of concentrating sunlight on flat plates," in *The Conference Record of the Twenty-Second IEEE Photovoltaic Specialists Conference - 1991*, vol. 1, pp. 586–592, Oct 1991.

[28] J. Meydbray and F. Dross, "Pv module reliability scorecard report," tech. rep., DNV GL, Norway, 2016.

[29] V. Poulek, D. Strebkov, I. Persic, and M. Libra, "Towards 50years lifetime of pv panels laminated with silicone gel technology," *Solar Energy*, vol. 86, no. 10, pp. 3103 – 3108, 2012.

[30] S. Bae, W. Oh, K. Lee, S. Kim, H. Kim, N. Park, S. Chan, S. Park, Y. Kang, H. Lee, and D. Kim, "Potential induced degradation of n-type crystalline silicon solar cells with p front junction," *Energy Sci Eng*, vol. 30, 07 2017.

[31] H.-L. Tsai, C.-S. Tu, and Y.-J. Su, "Developmennt of generalized photovoltaic model using matlab/simulink," *Proceedings of the World Congress on Engineering and Computer Science, San Francisco, CA, USA*, 2008.

[32] H. Tian, F. Mancilla-David, K. Ellis, E. Muljadi, and P. Jenkins, "A cell to module to array detailed model photovoltaic panels," *Sciverse ScienceDirect*, 2012.

[33] H. Ibrahim and N. Anani, "Variations of pv module parameters with irradiance and temperature," *Energy Procedia*, vol. 134, July 2017.

[34] G. Cibira, "Relations among photovoltaic cell electrical parameters," *Applied Surface Science*, vol. 461, pp. 102–107, 2018.

[35] D. Cotfas, P. Coftas, and S. Kaplanis, "Methods to determine the dc parameters of solar cells: A critical review," *Renewable and Sustainable Energy Reviews*, no. 28, pp. 588–596, 2013.

[36] X. H. Nguyen and M. P. Nguyen, "Mathematical modelling of photovoltaic cell/module/arrays with tags in matlab/simulink," *Environmental Systems Research*, 2015.

[37] M. F. Habbati Bella, Ramdani Youcef, "A detailed modeling of photovoltaic module using matlab," *NRIAG journal of Astronomy and Geophysics*, 2014.

[38] C. W. Hansen, "Parameter estimation for single diode models of photovoltaic modules," tech. rep., Sandia National Laboratories, Albuquerque, New Mexico 87185 and Livermore, California 94550, 2015.

[39] A. Senke and R. Eke, "A new method to simulate photovoltaic performance of crystallins silicon photovoltaic modules based on datasheet values," *Renewable Energy*, vol. 103, pp. 58–69, April 2017.

[40] K.-i. Ishibashi, Y. Kimura, and M. Niwano, "An extensively valid and stable method for derivation of all parameters of a solar cell from a single current-voltage characteristic," *Journal of Applied Physics*, vol. 103, no. 9, p. 094507, 2008.

[41] W. D. Soto, S. Klein, and W. Beckman, "Improvement and validation of a model for photovoltaic array performance," *Solar Energy*, vol. 80, no. 1, pp. 78 – 88, 2006.

[42] H. Maammeur, A. Hamidat, and L. Loukarfi, "A numerical resolution of the current-voltage equation for a real photovoltaic cell," *Energy Procedia*, vol. 36, pp. 1212 – 1221, 2013. TerraGreen 13 International Conference 2013 - Advancements in Renewable Energy and Clean Environment.

[43] P. Choubey and A. Oudhi, "A review: solar cell current scenario and future trends," *Recent Research in Science and Technology*, vol. 4, pp. 99–101, 2012.

[44] A. D. Rajapakse and D. Muthumuni, "Simulation tools for photovoltaic system grid integration studies," in *2009 IEEE Electrical Power Energy Conference (EPEC)*, pp. 1–5, Oct 2009.

[45] A. Jain and A. Kapoor, "A new method to determine the diode ideality factor of real solar cell using lambert w-function," *Solar Energy Materials and Solar Cells*, vol. 85, no. 3, pp. 391 – 396, 2005.

[46] M. Bashahu and P. Nkundabakura, "Review and tests of methods for the determination of the solar cell junction ideality factors," *Solar Energy*, vol. 81, no. 7, pp. 856 – 863, 2007.

[47] A. Laudani, F. R. Fulginei, and A. Salvini, "Identification of the one-diode model for photovoltaic modules from datasheet values," *Solar Energy*, vol. 108, pp. 432–446, 2014.

[48] J.Casbestany and L.Castaner, "A simple solar cell series resistance measurement method," *Revue de Physique Appliquee.*, 1983.

[49] R. G. Ross, Jr., "Flat-plate photovoltaic array design optimization," in *14th Photovoltaic Specialists Conference*, pp. 1126–1132, 1980.

[50] A. discussion on future trends in renewable energy and photovoltaics, Sep 2018.

Appendix

Apendix A

Matlab Codes for Thévenin equivalent circuit model

```
R_guess = 1;
R_guess2 = ones(20,1);
for j=1:20
   if (j>1)
      R_guess2(j) = R_guess2(j-1);
  end
  sim('thevenequa_Osigwe_modified_Winstead',1)
  % cap_voltage.time contains vector of time data
  % cap_voltage.data contains vector of signal data
v_max = max(cap_voltage.data);
 c1 = 0;
 c2 = 0;
 for i=1:floor(length(cap_voltage.time)/2)
 if ((cap_voltage.data(i) >= 0.2*v_max) && (cap_voltage.data(i) <= 0.8*v_max))
         c1=c1+1;
   end
```

```
end
  for i=floor(length(cap_voltage.time)/2) + 1:length(cap_voltage.time)
  if ((cap_voltage.data(i) >= 0.2*v_max) && (cap_voltage.data(i) <= 0.8*v_max))
        c2=c2+1;
     end
 end
  if (c1 > c2)
       R_guess2(j) = R_guess2(j) + 1;
  else
      R_guess2(j) = R_guess2(j) - 1;
  end
 R_guess = R_guess2(j);
end
plot(R_guess2)
```

Appendix B

```
Matlab codes varying Irradiance and Temperature\\
clear all
close all
%declaring variables
T=302;
Tr=298;
%Tr1=40;
ki=0.00023;
Iscr=3.75;
```

```
%Irs=0.00021;
A=1.3;
Ego=1.166;
alpha=0.473;
beta=636;
G= [1000 800 600 400 200];
k= 1.38065*10^(-23);
q= 1.6022*10^(-19);
Eg= Ego - (alpha*T*T)/ (T+beta)*q;
voc=22.5;
Np=3;
Ns=54;
vt=(Ns*k*T)/q; %thermal voltage
vo = [0:1:300];
ww=(exp(voc/(A*vt)))-1;
Irs=Iscr/ww; %reverse saturation current

finding values for all 5 values of sun
for i =1:5
    Iph= (Iscr+ki*(T-Tr))*((G(i))/1000); %phase current
    Io= Irs*((T/Tr)^3)*exp(q*Eg*((1/Tr)-(1/T))/(k*A));% saturation current
    I= Np*Iph-Np*Io*(exp(q/ (k*T*A) *vo./Ns)-1); %output
    P= vo.*I; %output power
    figure(1) %voltage vs current plot
    plot (vo,I);
    axis ([0 50 0 20]);
```

```
    xlabel('voltage in volts');
    ylabel('current in Amps');
    hold on;
    figure(2) %voltage vs power plot
    plot (vo,P);
    axis([0 50 0 500]);
    xlabel('voltage in volts');
    ylabel('power in watts');
    hold on;
    figure(3) %current vs power plot
    plot (I,P);
    axis([0 20 0 500]);
    xlabel('current in Amps');
    ylabel('power in watts');
    hold on;
end

Varying temperature
clear all
close all
%declaring variables
T= [302 308 313 318 323];
Tr=298;
%Tr1=40;
ki=0.00023;
Iscr=3.75;
```

```
%Irs=0.00021;
A=1.3;
Ego=1.166;
alpha=0.473;
beta=636;
G= 800;
k= 1.38065*10^(-23);
q= 1.6022*10^(-19);
voc=22.5;
Np=3;
Ns=54;
vo = [0:1:300];

%Eg= Ego - (alpha*(T(i))*(T(i)))/ ((T(i))+beta)*q;

for i=1:5

    vt=(Ns*k*(T(i)))/q; %thermal voltage
    ww=(exp(voc/(A*vt)))-1;
    Irs=Iscr/ww; %reverse saturation current
end


% finding values of varying temperatures
for i =1:5
    Iph= (Iscr+ki*((T(i))-Tr))*((G)/1000); %phase current
```

```
    Io= Irs*(((T(i))/Tr)^3)*exp(q*Ego*((1/Tr)-(1/(T(i))))/(k*A));% satur current
    I= Np*Iph-Np*Io*(exp(q/ (k*(T(i))*A) *vo./Ns)-1); %output
    P= vo.*I; %output power
    figure(1) %voltage vs current plot
    plot (vo,I);
    axis ([0 30 0 10]);
    xlabel('voltage in volts');
    ylabel('current in Amps');
    hold on
    figure(2) %voltage vs power plot
    plot (vo,P);
    axis([0 30 0 250]);
    xlabel('voltage in volts');
    ylabel('power in watts');
    hold on;
end
```

Appendix C

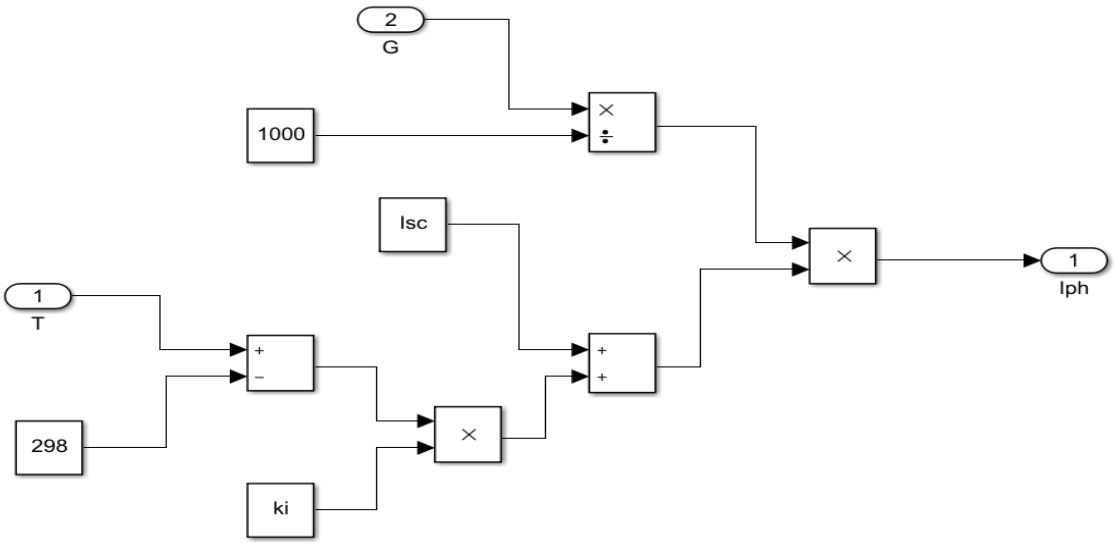

Figure 4.4: Modeled circuit for photocurrent

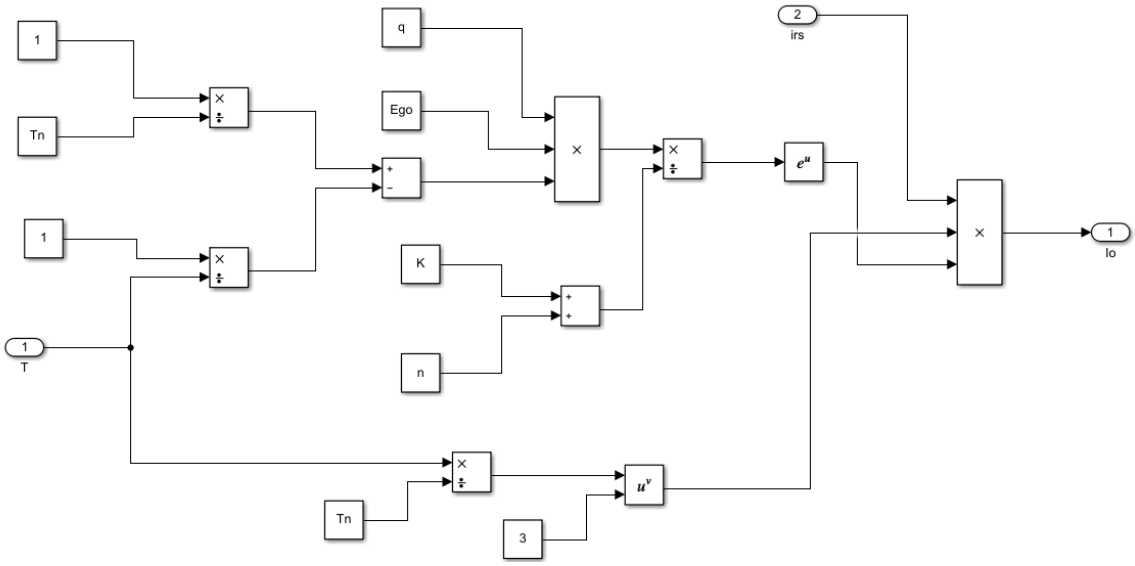

Figure 4.5: Modeled circuit for saturation current

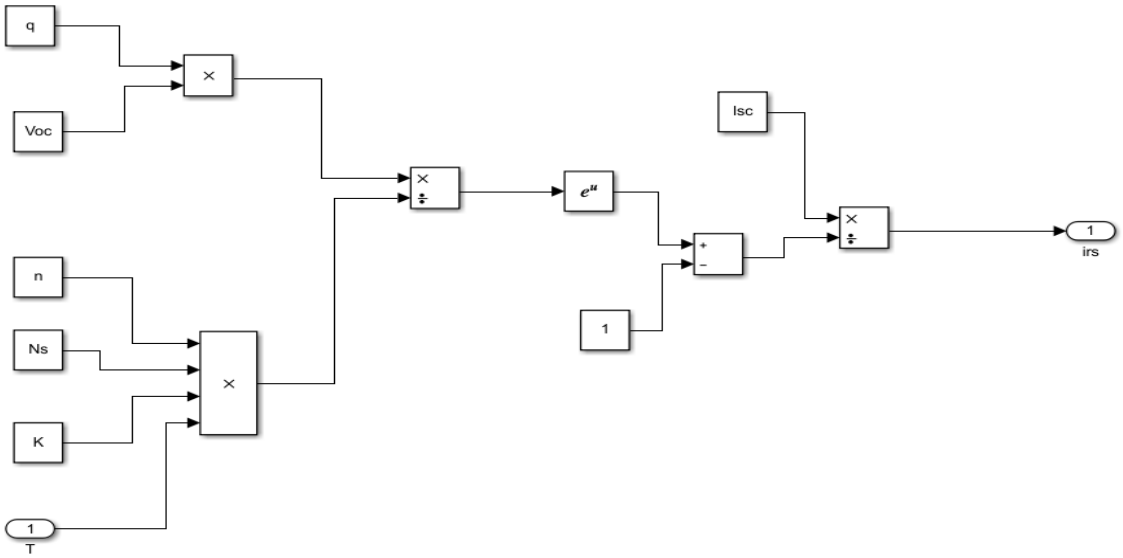

Figure 4.6: Modeled circuit for reverse saturation current

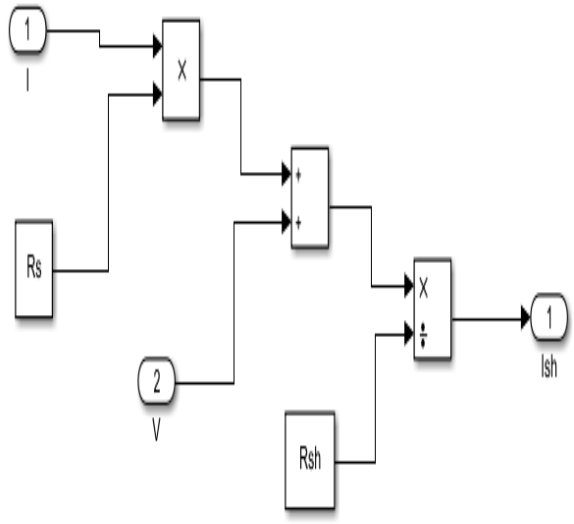

Figure 4.7: Modeled circuit for current through the shunt resistor

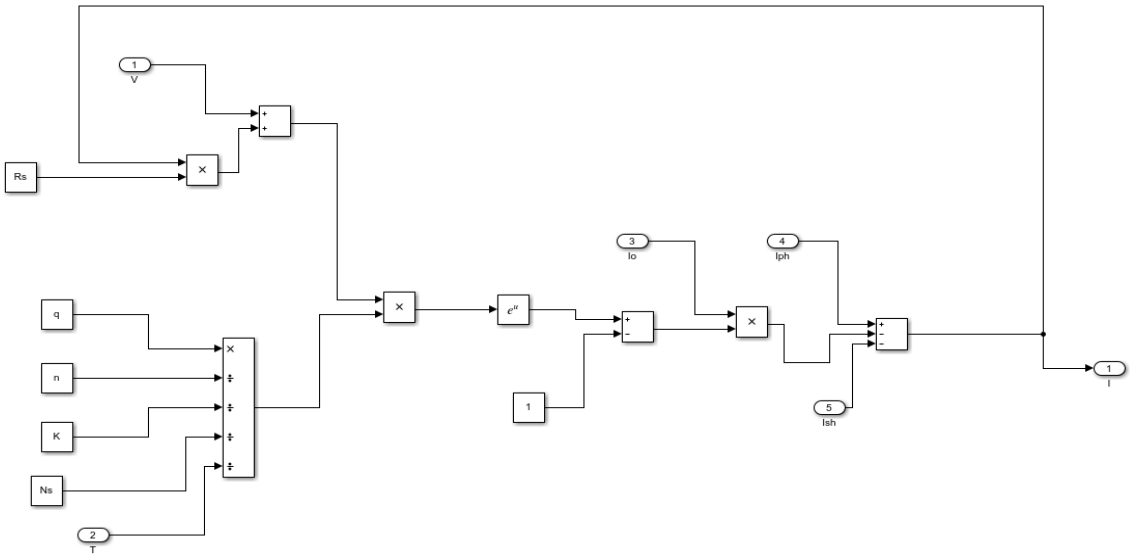

Figure 4.8: Modeled circuit for PV current